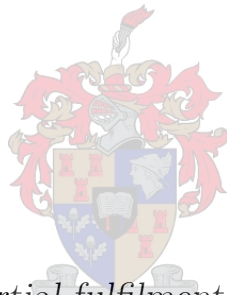# Simulation of flow inside the storage tank and piping of a thermosyphon type solar water heater

by

Tinus von Gericke Fourie

Thesis presented in partial fulfilment of the requirements for the degree of Master of Engineering (Mechanical) in the Faculty of Engineering at Stellenbosch University

Supervisor: Mr R.T. Dobson

March 2016

Declaration

By submitting this thesis electronically, I declare that the entirety of the work contained therein is my own, original work, that I am the sole author thereof (save to the extent explicitly otherwise stated), that reproduction and publication thereof by Stellenbosch University will not infringe any third party rights and that I have not previously in its entirety or in part submitted it for obtaining any qualification.

March 2016

Date: . . . .

i

Abstract

Simulation of flow inside the storage tank and piping of a thermosyphon type solar water heater

T.V.G. Fourie

Department of Mechanical and Mechatronic Engineering,
University of Stellenbosch,
Private Bag X1, Matieland 7602, South Africa.

Thesis: M.Eng (Mech)

March 2016

Even though Southern Africa has some of the highest solar resource in the world, solar water heaters are not as widely implemented as elsewhere on the planet. Reasons for this include the high upfront costs. Also, a possible opportunity for job creation is missed since the majority of currently installed systems are imported from abroad. In an attempt to encourage research among Southern African students and development within industry, the question was posed: How well can a one-dimensional, finite-volume computational model derived from first principle capture the flow inside a thermosyphon type solar water heater? Two such models are here developed and validated. The first simulates flow inside the thermosyphon loop. The second simulates the hot water storage tank by modelling plume formation and entrainment. By comparison with experimental data, it was found that the thermosyphon loop model corresponds well, while improvement is encouraged on the plume model. This considered, it was the conclusion that a one-dimensional, finite-volume model can indeed capture the flow within a thermosyphon type solar water heater.

Uittreksel

Simulasie van vloei binne die water tenk en die pype van 'n natuurlike-vloei-tipe sonkrag warmwatertoestel

("Simulation of flow inside the storage tank and piping of a thermosyphon type solar water heater")

T.V.G. Fourie

Departement Meganiese en Megatroniese Ingenieurswese,
Universiteit van Stellenbosch,
Privaatsak X1, Matieland 7602, Suid Afrika.

Tesis: M.Ing (Meg)

Maart 2016

Suider-Afrika het van die rykste son hulpbronne op die planeet. Ten spyte van hierdie feit word sonkrag warmwatertoestelle nie so baie gebruik soos in ander streke nie. 'n Moontlike rede hiervoor is die duur aanvanklike koste. Nog 'n belangrike aspek is dat meeste van hierdie toestelle nie in Suider Afrika vervaardig word nie. Talle werke wat sou kon geskep word daardeur lei hieronder. Om dus verdere navorsing onder beide studente en in industrie aan te moedig, word hierdie vraag gestel: How goed kan 'n eendimensionele, eindige-volume rekenaarmodel die vloei binne 'n natuurlike-vloei-tipe sonkrag warmwatertoestel vasvang? Twee sulke modelle word hier ontwikkel. Die een behels die vloei in 'n natuurlike-vloei-lus. Die ander simuleer pluim-vorming binne 'n warmwater tenk. Dit is bevind dat die eerste model goed korreleer met eksperimentele resultate, terwyl die tweede verbetering verg. Nietemin is die finale bevinding dat 'n eendimensionele, eindige-volume rekenaarmodel wel die vloei binne 'n natuurlike-vloei-tipe sonkrag warmwatertoestel vasvang.

Acknowledgements

I would like to express my sincere gratitude, first and foremost, to my Lord. I also thank my supervisor, Mr R. T. Dobson, my understanding flatmates and family and Mr C. Beldon for his assistance with the experimental work.

Dedications

To C.R.B. Von Gericke

Contents

List of Figures

LIST OF FIGURES ix

Nomenclature

A Control volume cross-sectional area

A_t Tank control volume cross-sectional area

A_z Control volume circumferential area

C_f Fanning friction factor

c_p Specific heat capacity

D Diameter

F Force in the flow direction

g Gravitational acceleration ($g = 9{,}81$)

h Specific enthalpy

h_{conv} Convective heat transfer coefficient

h_f Frictional head losses

h_l Head losses

h_l^* Adjusted head losses

h_m Minor head losses

h_{th} Thermosyphon driving head

K_{L} Minor loss coefficient

k Thermal conductivity

L_c	Characteristic length
M	Adjustment factor used to calculate h_l^*
$\dot{m}$	Mass flow rate
Nu	Nusselt number
P	Pressure
$\dot{Q}$	Heat flow rate
R	Thermal resistance
Re	Reynolds number
r	Inside radius
T	Temperature
v	Velocity
z	Co-ordinate
α	Entrainment coefficient
Δh	Change in specific enthalpy over time
Δm	Change in mass over time
ΔP_l	Pressure drop due to major and minor losses
ΔP_{th}	Pressure rise due to the thermosyphon driving head
Δt	Time-step size
Δz	Control volume height
ϵ	Emissivity
σ	Stefan-Boltzmann Constant
μ	Viscosity

ρ Density

τ Shear stress

Chapter 1

Introduction

1.1 Background

Among the many advancements of solar energy, a resource Southern Africa has plenty of, the usage of solar water heaters have enjoyed much attention. The harnessing of the sun's radiation, not to generate electricity, but directly as thermal energy, is one of the most effective implementations to date.

Many versions of the solar water heater have been developed. The basic components of all of the variations are similar, however. These are the solar collector (hereafter just referred to as the collector), the hot water storage tank (HWST) and the piping connecting the two. These components are shown in Figure 1.1.

The *collector* is especially designed to collect radiation from the sun and transfer the heat to a working fluid flowing through it. Main variations include a flat plate collector and evacuated tubes.

A flat plate collector, literally a painted metal plate connected to several pipes of working fluid, is by far the simpler of the two, but also looses more heat to the ambient air. This heat loss can be reduced by placing the pipes of working fluid inside transparent evacuated tubes. These collectors have significantly lower thermal losses, but slightly increased optical losses. This is because the solar radiation has to pass through the external transparent tube before it can reach the collector itself. These devices are also more expensive than simple flat plates.
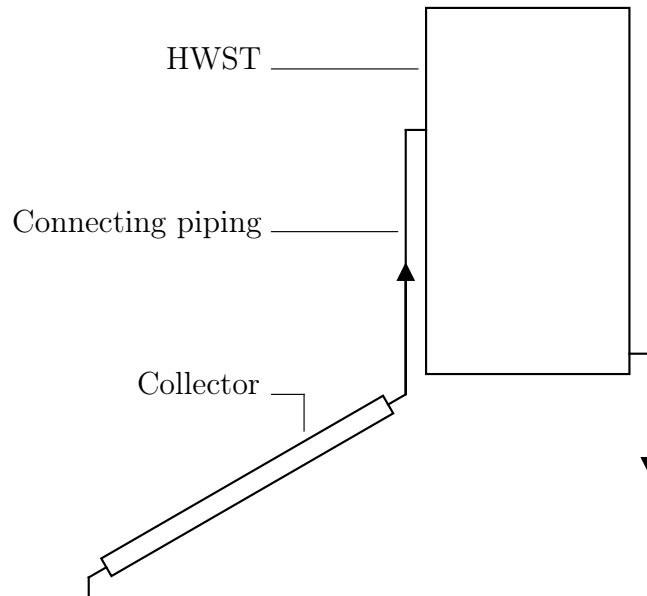
Figure 1.1: Components of a solar water heater

Although not used in solar water heating systems considered here, a third possible type of collector exists. It is even simpler that the flat plate and consists only of dark collector tubes. This is almost exclusively used to heat swimming pools.

Whichever collector is used, the heat it absorbs from the sun is stored in the *HWST*. These tanks are insulated to prevent heat loss. They too occur in various shapes and sizes, with the main distinction being between horizontal and vertical tanks.

As far as the *connecting piping* is concerned, many possibilities are also in use. The first distinction can be made between the standard solar water heating system depicted in Figure 1.1 and what is termed the *Integrated Collector Storage Solar Water Heater* (ICSSWH). In the standard system, the collector and storage tank are physically separate from one another and connected only by piping. The collector could, for instance, be placed on the roof and the HWST in the basement of a house. In contrast to this, the ICSSWH is built as a single physical unit, with only an internal wall separating the collector from the storage tank. This is shown in Figure 1.2.

The standard system (in which the collector and HWST are physically separate, as shown in Figure 1.1) can be further divided into direct and indirect,
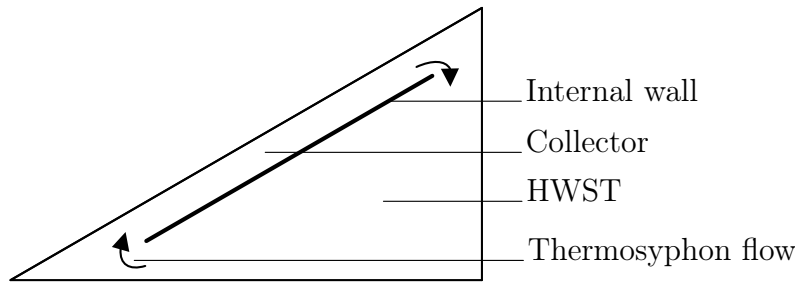
Figure 1.2: Diagram of an Integrated Collector Storage Solar Water Heater

as well as, pumped or natural circulation system.

In a direct system, the working fluid flowing through the collector is directly stored in the HWST. This is the simplest variation.

In some climates, however, extremely low temperatures necessitate the use of antifreeze in the working fluid. This anti-freeze-containing working fluid cannot be stored in the tank and distributed to the household the system serves. It therefore passes from the collector to a heat exchanger inside the HWST and back to the collector. In this heat exchanger, the working fluid transfers its heat to the water in the HWST. The collector–tank–collector loop is thus completely separate from the cold-water-mains–tank–hot-water-load loop. A system such as this is referred to as an indirect system.

Lastly, the working fluid can either be pumped within its loop, requiring an input of electricity, or be driven by natural circulation. In a natural-circulation-driven system, knows as a thermosyphon type solar water heater, the difference in density between the working fluid in different parts of the system drives the flow. As shown in Figure 1.3, the fluid inside the collector is hotter than that in the tank and "down-comer tube" and is consequently less dense. Therefore, this "lighter" fluid rises due to buoyancy, while the pressure causes the heavier fluid to fall, resulting in natural circulation.

An obvious advantage of a thermosyphon type system over its pumped counterpart is that no electricity is needed for pumps. However, for the thermosyphon effect to be useful, certain restrictions are placed on the design of the system. For instance, the HWST must be above the collector. These restrictions are not imposed on a pumped system.

These variations in configuration exists largely because of different require-
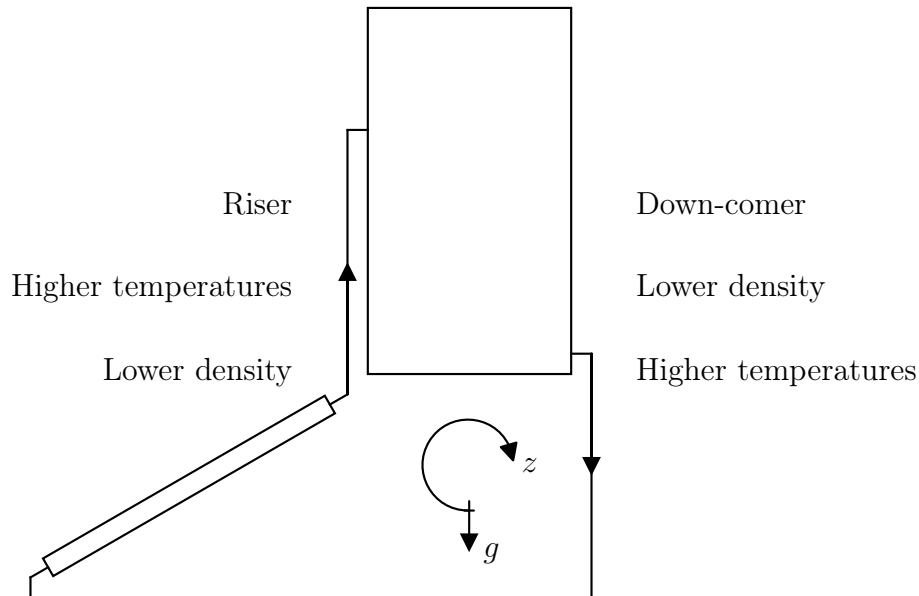
Figure 1.3: Thermosyphon flow

ments in different locations. Also, because the initial development of these systems were done largely by trial and error (Morrison and Braun, 1985) and to a lesser extent because of scientific design and understanding.

In contrast, the present research will focus on understanding and developing some of the mathematics that form a part of one specific configuration.

1.2   Research question

From the description of the various components of a solar water heater, it can now be seen that the system shown in Figure 1.1, most closely resembles a direct thermosyphon type solar water heater with a vertical HWST. It is this configuration that is discussed in this thesis.

More specifically, it is the HWST and connecting piping that will be studied and mathematically modelled. This investigation, focussing on these two components, will attempt to answer the following research question:

> *How well can a one-dimensional, finite-volume, computational model capture the flow inside the storage tank and piping of a thermosyphon type solar water heater?*

1.3   Significance and motivation

Is shall be noted that the solar collector itself will not be modelled as a part of this study. This is since the present thesis form part of a larger research undertaking.

At it's heart, the motivation behind this larger project is found in an attempt to invest in Southern Africa.

This region has some of the highest values of annual solar insulation on the planet. Yet, it is by no means a leader in either the production or implementation of solar water heaters. This technology, which has the potential to positively impact the population's socio-economic situation, is being underutilised.

South African Energy Minister in 2009, Dipuo Peters, launched a program to implement 1 million solar water heaters nationwide. In the launching speech, it was stated that 100 000 jobs would be created in the process (Wlokas and Ellis, 2013).

Contrast this to the estimated 5 900 jobs sustained by the industry in 2003 (Austin *et al.*, 2003). This number had not risen much by 2011, largely because of slower implementation, a shortage of training and expertise and loss of manufacturing jobs, according to Wlokas and Ellis (2013). This is since most jobs are created during manufacturing, and the majority of currently installed solar water heaters are imported from China.

Also, according to a study done by Austin and Morris (2005), the main reasons for the lack of implementation lies in the high upfront cost, inability to afford this due to poverty and a bad public perception about the technology. (Even though the pay-back period of current devices make them economically feasible, it is the initial capital expenditure that is not as widely affordable in the region due to poverty.) To better utilise the Southern African solar resource using solar water heaters, these matters thus have to be addressed.

Both could potentially be solved by the same action: the development of a solar water heater optimised for Southern African conditions.

Such an optimised device should be manufacturable locally from Southern African materials and designed for Southern African conditions. The increased

amounts of radiation this region receives as compared to Germany and China (where the majority of currently available devices originate) allows for simpler and cheaper designs. In this way, the upfront cost could potentially be reduced and more jobs created in the process.

This emphasis on Southern African conditions is what suggests the use of the thermosyphon type water heater. Though many variations have emerged as has been previously discussed, the thermosyphon type solar water heater has been widely implemented due to its simplicity and economic viability (Ziapour and Aghamiri, 2014).

It is also the configuration that requires the least amount of maintenance and is the simplest to manufacture. It does not have the electrical pump losses associated with pumped systems and does not require sophisticated control systems. All of this contribute to the desired simplicity of the intended optimised design.

In order for such a design to be successful, it would need to be as simple as possible. Simple to understand, manufacture, operate and maintain.

A simple one-dimensional, finite-volume model could potentially encourage the development of this optimised design. It could promote the understanding of flow inside a solar water heater among under-graduate level engineering students and encourage the optimisation of possible designs among postgraduates. It could be used in industry to reliably predict the performance of these systems and grant more surety to potential new customers.

Such a model would have to be easily adaptable and expandable and be able to accommodate various changes in the design. Such changes might include different collector configurations or hot water draw off strategies. However, all alterations are likely to incorporate two important components: the piping network and the HWST.

Those two component will be the subject of this thesis. It is upon them that the model to be developed in the remainder of the larger project is to be based. In short, it is hoped that the outcome of the present research question will seed more research and development as a part of this larger project.

1.4   Research goals and objectives

The present research question thus forms part of a larger project aimed at the development of a solar water heating system optimized for Southern African conditions.

Towards this end, the following research goals and accompanying objectives have been set:

Goal 1 Develop a one-dimensional, finite-volume, computational model of the piping network and HWST of a thermosyphon type solar water heater

      i Model the thermosyphon loop

     ii Model the hot water storage tank

Goal 2 Establish the validity of the model

      i Investigate proper validation techniques

     ii Compare the computational model to experimental results

Goal 3 Encourage future research into the development of a solar water heating system optimised for Southern African conditions

      i Ensure that all models are simple and easy for undergraduate level engineering students to understand

     ii Develop all models modularly to ensure that they are easy to expand

By reaching these objectives and goals, the research question will be answered, and underlying mission of seeding additional research accomplished.

1.5   Scope and limitations

The accomplishment of these goals will not, however, lead to a complete model of a thermosyphon type solar water heater. It is not the purpose of the present research to develop the entire model. The present research question involves only an investigation into the legitimacy of using a simple one dimensional approach to create the model. Specifically, only the thermosyphon loop and

the hot water storage tank will be modelled in detail. To further ensure the simplicity of these initial models, some further limitations are applied.

Most importantly, the two sub-models to be developed (the piping system, or thermosyphon loop, and tank models) will be based on a simplified experimental set-up. In other words, the models will attempt to simulate the flow inside the experimental set-up and not the general case of a functioning solar water heater.

This limitation is imposed to allow for the two models to be separately validated under laboratory conditions. It is also in accordance with the stated objective of comparing the computational model to experimental results.

For the same reasons, the collector will be treated as a simple source of constant heat flux. In the experimental set-up, this will be accomplished by using an electrical element. Also, only vertical storage tank will be considered for simplicity.

Finally, as far as possible, references and correlations that are available to undergraduate students will be applied. This is to aid in the accomplishment of the objective of ensuring the models are understandable at an undergraduate engineering level. This limitation will be freely neglected, however, if the correlations available in undergraduate references are not applicable.

1.6   Thesis overview

With these limitations established, the remainder of this document details the process followed towards reaching the stated goals and objectives.

In Chapter 2, the methodology to be used to reach Goals 1 and 2 will be discussed. This includes the philosophy behind the development of the models as well as the verification and validation procedures to be followed. This chapter also elaborates on how the manner in which this research is done will contribute towards the reaching of Goal 3 above, the encouragement of future research.

Chapter 3 introduces the experimental set-up. This short chapter is included early, since it is upon this set-up that the two computational models are based.

Chapters 4 and 5 will elaborate upon these two models themselves, namely the thermosyphon loop and the hot water storage tank, respectively. Each chapter will include a study of literature, a detailed mathematical development of the model and a discussion about the verification and validation thereof.

Finally, Chapter 6 concludes the document and offers several recommendations.

Chapter 2

Research design and methodology

At its core, the research question here discussed involves the development, verification and validation of computational models and simulations. A review on published literature regarding these processes is presented in this chapter, as well as a discussion on the specific design chosen for the present research.

2.1   Model creation methodology

According to Sargent (1981), the model development process can be simplified into the following three components and the tasks relating them:

- The actual, real world, *system* under consideration,

- The mathematical or *conceptual model* describing it, and

- The *computerised model* which is an implementation of the conceptual model into executable code. The execution of this code is then known as a simulation of the system.

These components and their relating processes are depicted in Figure 2.1.

The real world system is analysed and modelled, resulting in simplified mathematical descriptions of what is happening in the physical world. Although this conceptual model is often based upon theory previously developed and published, the implementation of that theory is not guaranteed as correct. Nor is

the assumptions inherent in simplifying the system into conceptual mathematics. This uncertainty necessitates what is know as *conceptual model validation.* (All forms of validation and verification will be discussed in the next section.)

Once the conceptual model is proven valid, it needs to be translated into a computer program. Additional verification is then required to ensure that the computer program does indeed perform the task the conceptual model intends.

Finally, the computerised model is to be validated against the actual system by experimentation, a process known as operational validation.
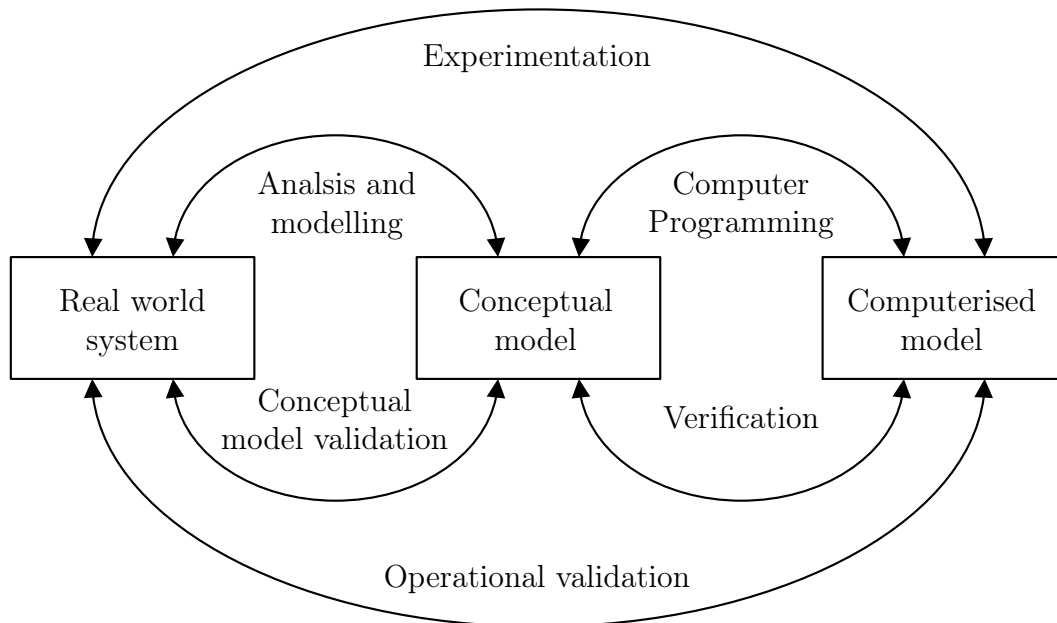
Figure 2.1: The simplified model development process

This methodology is partially based on a system know as multi-stage validation, developed by Naylor and Finger (1967). According to the multi-stage philosophy, model development includes three phases...

Rationalism The analyses and modelling of a system based on sound science: proven theory, recorded observations and general knowledge

Empirical validation The testing of assumptions inherent in the model by experimentation

Positive economics The comparison of the input-output relationships of the system and computerised model

It can be seen from Figure 2.1 how these phases relate to the simplified model development process. Rationalism forms part of analyses and modelling, while empirical validation and positive economics relate to validating the conceptual and computerised model's correctness.

The multi-stage philosophy of Naylor and Finger (1967) does not explain the programming or computerised model verification phases, however. These processes, Sargent (1981) advises, are to be performed using the techniques proven successful in software engineering. Chapman (1998) and Maclaren (2010) introduces some such methods.

According to Chapman (1998), the creation of a computerised model involves

Step 1 Stating the problem,

Step 2 Defining inputs and outputs,

Step 3 Describing the algorithm to be utilised (gradually decomposing the main problem into smaller and smaller parts in a stepwise, top-down decomposition),

Step 4 Writing the required code to perform the algorithm and

Step 5 Testing the final product.

Steps 1 to 3 readily corresponds to the creation of a conceptual model, as outlined in the simplified process of Sargent (1981), while step 5 reflects computerised model verification.

Maclaren (2010) echoes these ideas. He emphasises that a program is to be broken down into simpler functions (as in step 3). Also, that the specific task of each function is to be clearly stated and its inputs and outputs defined (as in steps 1 and 2). Maclaren (2010) further emphasises the proper commenting of all code and the inclusion of error checking – ensuring bounded inputs and outputs – into the code itself (thereby elaborating upon step 4). Lastly, he

states that each function is to be separately tested (mirroring step 5). This separate testing of all sub-units of a program is known as unit testing.

These software development methods, along with the simplified model development process, are all to be employed in developing the one-dimensional computerised model required to answer the current research question.

2.2 Model validation and verification methodology

With a computerised model developed as described by the above authors, steps can now be taken to ensure its validity.

Anshoff and Hayes (1973) reasoned that the more confidence a user has in a model, the greater the value of the model. This confidence, however, is undermined by uncertainties arising from various sources. According to Roy and Oberkampf (2011), three main sources for this uncertainty exist. These are uncertainties due to model input, numerical approximation and model form.

Model form refers to the assumptions an approximations applied to simplify a physical phenomenon to mathematical form. Loosely put, this refers to the mathematical equations used to model the system. These assumptions and equations can easily be erroneous.

Even if the assumptions and mathematics is absolutely perfect, though, the final model can still be wrong due to the numerical implimentaion of the mathematics. For example, when modelling a mathematical derivative as a finite difference over a finite time the error involved can easily become excessive.

Finally, even if both the mathematics and numerical implementation is flawless, the model input can still be incorrect and will thus result in an incorrect output. Model input here involves the geometry, parameters and boundary conditions of a model. The results predicted by a model may, for instance, be false due to an incorrect measurement used to build the model.

To further complicate the matter, it is often not known from which of these sources an error originates. Also, a fault resulting from one of these might, in

a certain case, cancel a fault from another, producing what seems to be correct results, which, in fact, are not.

It can thus be seen that to obtain increased levels of confidence, the cost of both model development and especially validation procedures greatly increase. It is therefore imperative to know what the purpose of the model is and what level of accuracy is required for it to be useful.

This, for the present model is simple: to encourage research. Though greater confidence will be the result of later models, it is not presently required. For the present model to closely resemble experimental results is confidence enough.

With this established, a methodology of validation and verification can be further explored.

As shown in Figure 2.1, ensuring that a model is accurate involves three processes,

- Conceptual model validation,

- Computerised model verification and

- Operational validation

The middle step, that of *verification*, is concerned with ensuring that the computerised model – the code written in some programming language – is a correct implementation of the conceptual model.

Validation, on the other hand, is about determining whether both the conceptual and computerised models correctly reflect reality. Sargent (2013) defines validation as "substantiation that a model within its domain of applicability possesses a satisfactory range of accuracy consistent with the intended application of the mode." The final product of proper validation is thus the assurance that a model is an accurate enough prediction of the real world to be useful in its intended purpose.

Conceptual model validation involves ensuring that the model assumptions and mathematical treatments are correct. It thus deals with the model form uncertainty discussed above.

Since the conceptual model is rarely capable of producing data before it is computerised, statistical test cannot be performed on its input-output relationships. However, its underlying assumptions and theory can often be tested and validated experimentally. Also, the combination of these assumptions and theory into a complete model can be validated using a subjective technique known as *face validation*.

This is a method in which experts in a field evaluate the correctness of a conceptual model based on personal experience (Sargent, 1986). To accomplish this, the conceptual model is often depicted graphically. Examples include using a flowchart, structured walk-through or an animation. This then enables the experts to see the interaction of the various assumptions and theories (Sargent, 2013).

A variation upon the method of face validation is to base the model on assumptions and theories (and the interactions between these) which have already been proven in peer reviewed literature. Alterations to accepted models can thus more easily be explored, without explicit face validation. This is the method of conceptual model validation to be used in the present model: basing the model on accepted and previously proven assumptions.

The next process is that of verification, which deals with the numerical uncertainty previously discussed. It was already stated that a method of verification involves ensuring proper coding practice. The software development procedures discussed as part of modelling methodology is thus one way in which the present model with deal with verification. This especially includes unit testing.

Another verification technique involves comparing a computerised model's output with a known "correct" result (Oberkampf and Trucano, 2008). This is achieved by comparing simplified parts of the model with known exact solutions. The level of accuracy required for this technique is outside the purpose of the present model, however.

But, what will be implemented as another part of verification, is a grid and time-step independence study.

Lastly, with the conceptual model validated and the computerised implementation thereof verified, the computerised model itself is validated. This *Op-*

erational validation involves testing the input-output behaviours of the final computerised model. The most common method employed is comparing the results with both experimental data, as well as, the results obtained from other models.

If enough valid data is available, statistical methods such as hypothesis testing or confidence intervals can be used to make a objective decision about the model's validity. However, graphical representations such as graphs and charts can also be used to make a subjective decisioned about the quality of the model. If detailed precision is not an express requirement for the model to fulfil its purpose, this qualitative (vs quantitative) judgement is sufficient.

Since the purpose of this present model is to seed future research and to determine whether there is value in a one-dimensional, finite-volume model, the accuracy and precision required from it (at this point) is not that high. Graphical, subjective validatory techniques will thus be adequate and will therefore be used.

Chapter 3

Experimental set-up

Both the models (to be developed and validated according to the methods just discussed) will be based on the experimental set-up introduced in this chapter. This set-up and the experimental results it produces, will also be used to validate the models.

The experimental model is shown in Figure 3.1 below.

Figure 3.1: Experimental set-up

As can be seen from the figure, this set-up consists of a water storage tank and a loop of glass and pvc tubing. Within the glass tubes is contained a 3kW geyser element. This design was chosen to mimic the simplest case of the one-dimensional, finite-volume model.

Figure 3.2 shows the different parts of this model and its relation to an actual solar water heating system.
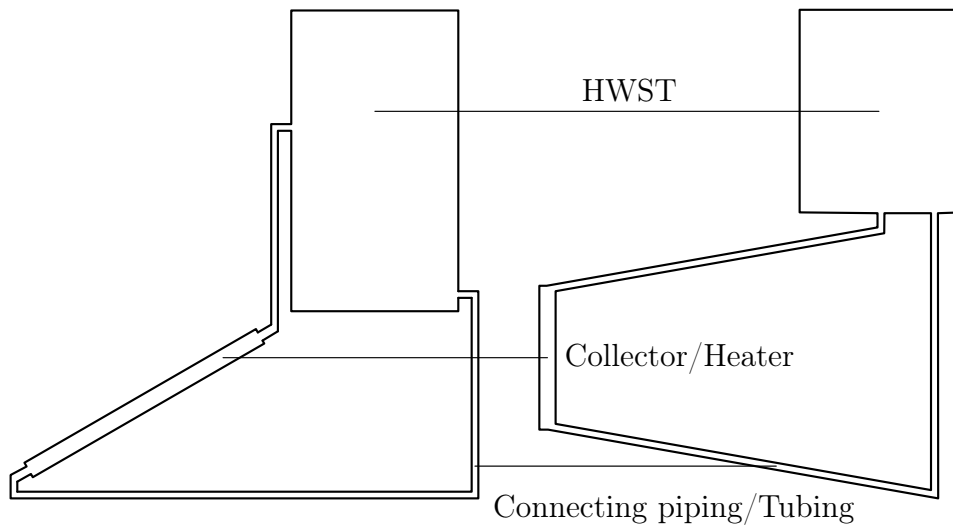
Figure 3.2: Solar water heating system vs simple model

In this model, the tank represents the HWST. Its inlet from the thermosyphon loop is situated in the centre of its base. The simple loop of tubing simulates the connecting piping while the geyser element, or heater, is a controlled way of simulating a solar collector. The heat input into the system is controlled using a variac.

Temperature measurements throughout the system were taken using ten (calibrated) T-type thermocouples, attached to an Agilent data acquisition unit and logger. The positions of these thermocouples are shown in Figure 3.3.

In addition to temperature data, the flow rate of the water in the loop had to be measurable in order to aid the validation procedures. This was accomplished by injecting small amounts of die into the flow using syringes. The injection points are shown in Figure 3.4

Also shown in this figure is a clearly marked 10 cm long section of the tubing. The flow rate was measured by manually measuring the amount of time it takes the fluid (and die mixture) to pass along this section of known length.
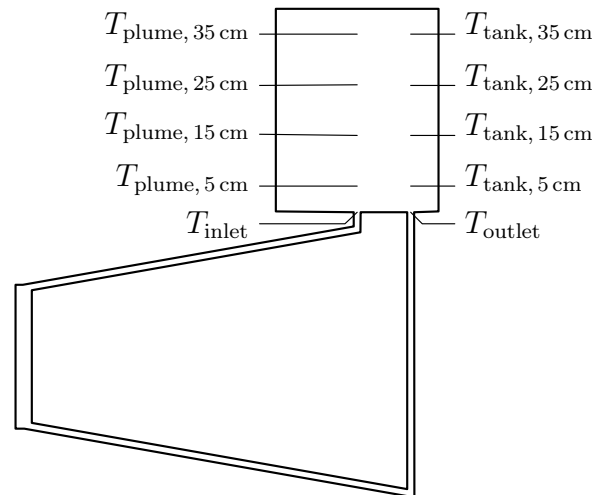
Figure 3.3: Thermocouple placement in the experimental set-up
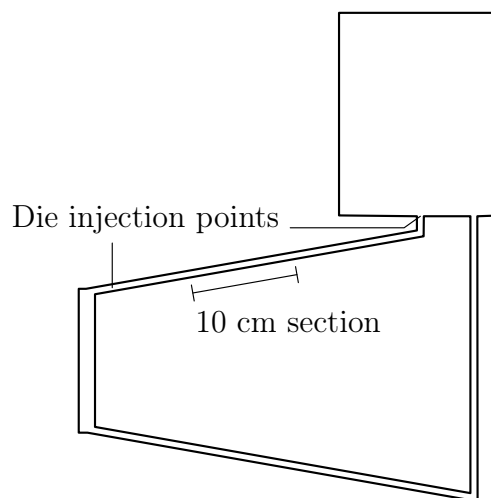
Figure 3.4: Die injection points in the experimental set-up

From the average velocity, the mass flow rate through the tube can then be found as

$$\dot{m} = \rho v_{\mathrm{avg}} A \tag{3.1}$$

where A is the cross sectional area of the tube. The density used in Equation (3.1) is the density at the known tank inlet temperature, T_{inlet} in Figure 3.3.

This set-up thus allows the measurement of key temperature and flow rate data. This was all that was required to effectively validate the two models.

Chapter 4

Thermosyphon loop

4.1   Literature survey

A great many natural phenomenon depends on buoyancy driven flow. Including the thermosyphon loop of a solar water heating system. The latter is, however, a complex occurrence. So much so that the first mathematical treatments only appeared in the 1970's and 80's. During this period, the work of several authors (Ong, 1974, 1976; Morrison and Ranatunga, 1980a,b; Morrison and Tran, 1984) greatly advanced the understanding and modelling of this type of flow. Their work lead to the development of the TRNSYS Type 45 component simulating thermosyphon flow (Solar Energy Laboratory, 2009), upon which the majority of new research focusses (Abdunnabi and Loveday, 2012).

This present project will focus not on the TRNSYS implementation, however. In accordance with the stated objective of ensuring continual research and especially encouraging understanding at an undergraduate level, the mathematics will be developed from first principle. Also, it will keep with the chosen validation methodology of basing the current model on accepted assumptions. The models developed by the aforementioned authors during the 1970's and 80's will therefore be discussed in detail, with the end goal of employing their assumptions in a modern model.

All of the surveyed models employ the same basic framework:

- The collector, hot water storage tank and connecting piping are modelled

as a single closed loop (as depicted in Figure 4.1)

- The new temperatures at each time-step are calculated using some form of the transient energy equation

- The fluid is assumed to be incompressible, except that varying density is taken into account only where it appears in the governing equations multiplied by g (the so called Boussinesq approximation).

- Fluid velocity or mass flow-rate is found by equating the thermosyphon and friction heads, according to Equation (4.1)

- This equation results from assuming quasi steady state as far as the momentum and continuity equations are concerned.
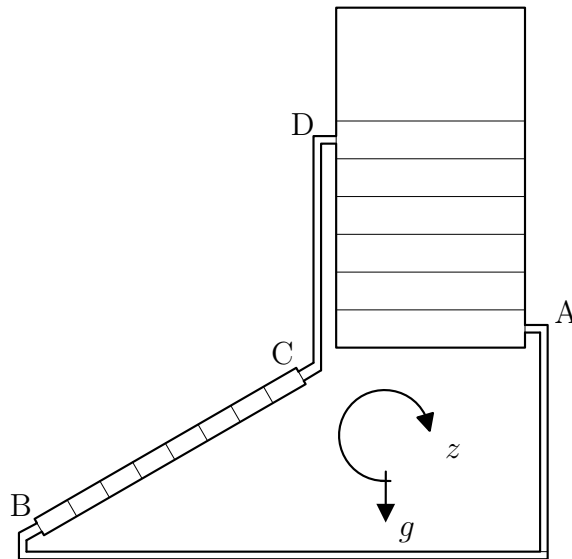
Figure 4.1: The modelled thermosyphon loop

The calculation of fluid velocity discussed above is based upon the equation

$$\mathrm{h}_{th} = \mathrm{h}_{l} \tag{4.1}$$

In this equation, h_{l} is the friction and minor losses head opposing flow, while h_{th} is the thermosyphon head driving it. Morrison and Ranatunga (1980a) found this thermosyphon head to be between 1 mm and 30 mm water.

Although the models differ slightly, they all essentially compute the thermosyphon head by individually integrating the down-comer and riser sections of the loop, resulting in

$$\mathrm{h}_{th} = \frac{\int_{DAB} \rho g \ \mathrm{d}z - \int_{BCD} \rho g \ \mathrm{d}z}{\bar{\rho} g} \tag{4.2}$$

where the limits of integration refer to the points depicted on Figure 4.1. This method, however, results in inaccurate calculation of reduced and reversed flow when the collector is not receiving the normal daytime levels of radiation.

Despite these stated similarities, the surveyed models do differ in many other aspects. Firstly, early models calculated the temperature dependent properties only once and at the expected mean transient temperature. These properties include collector efficiencies, heat transfer coefficients, friction factors and properties of water. Starting with the first model by Ong (1974), however, temperature dependent properties are recalculated for every new temperature at each time-step.

Secondly, the number of nodes used in the models vary. Ong (1974) performed an energy balance at each time-step *on the overall average temperature of the loop*. Effectively this model thus uses only one node. In contrast, Ong (1976) divides the loop into the control volumes depicted in Figure 4.1. Note that this scheme treats each section of the connecting piping as a single node. It does, however, include multiple control volumes along the length of the tank. Specifically, Ong (1976) used 10 tank control volumes, while Morrison and Tran (1984) used 20. Increasing the number of nodes was found to increase the accuracy of the model, but also required finer time-steps (Morrison and Tran, 1984).

Lastly, the main development that Morrison and Ranatunga (1980*a*,*b*) introduced is found in the calculation of the head losses, h_l. This is the sum of the frictional head, h_f, and other head losses due to fittings and bends, h_m. It is expressed as

$$\mathrm{h}_l = \sum \left(\frac{64}{\mathrm{Re_D}} \frac{1}{2r} + \frac{K_\mathrm{L}}{\Delta z} \right) \frac{v^2}{2g} \ \Delta z \tag{4.3}$$

In this equation, $\frac{64}{\text{Re}_\text{D}}$ is the Darcy–Weisbach friction factor (Çengel and Cimbala, 2010) for laminar flow. However, Morrison and Ranatunga (1980a,b) argued that the flow found in actual systems are often in the developing regime and not purely laminar. As a result, the resistance to flow due to friction is greater than is calculated in Equation (4.3).

To correct this error, they proposed the inclusion of the ratio M, defined as

$$M = \frac{\text{h}_{f,\text{ developing flow}}}{\text{h}_{f,\text{ laminar flow}}} \tag{4.4}$$

into Equation (4.3).

Morrison and Ranatunga (1980a,b) found the value of M to be

$$M = 1.0 + \frac{0{,}038}{(\Delta z/D\ \text{Re}_\text{D})^{0{,}96}} \tag{4.5}$$

Using this ratio, the adjusted head loss to be used in Equation (4.1) becomes

$$
\begin{aligned}
\text{h}_l^* &= \sum \left(\frac{64}{\text{Re}_\text{D}} \frac{1}{2r} M + \frac{K_\text{L}}{\Delta z} \right) \frac{v^2}{2g}\ \Delta z \\
&= \sum \left(\frac{64}{\text{Re}_\text{D}} \frac{1}{2r} \left(1.0 + \frac{0{,}038}{(\Delta z/D\ \text{Re}_\text{D})^{0{,}96}} \right) + \frac{K_\text{L}}{\Delta z} \right) \frac{v^2}{2g}\ \Delta z
\end{aligned}
\tag{4.6}
$$

This adjusted head loss will be used in the one-dimensional, finite-volume model to be developed in the next section.

This is in accordance with the chosen validatory technique of basing a new model on accepted assumptions and simplifications. It is towards this end that the discussed literature was surveyed.

In conclusion, therefore, the authors just discussed and the models they proposed have the following features significant to the current research.

- By modelling the system as a closed loop, many simplifications can be made.

- The transient energy equation can be used to calculate new temperatures at each new time-step.

- Temperature dependent properties (such as density) can then be calculated from the new Temperatures.

- To calculate new flow rates, the flow can be assumed to be at a steady state *at that time-step*. A quasi-steady state approach is thus used. According to this assumptions, the transient terms in the conservation of mass and momentum equations can be taken as zero.

- The conservation of momentum reduces to Equation (4.1) under these assumptions. This states that the thermosyphon driving head is opposed by the head losses due to friction and other minor losses.

- This head loss should be calculated for developing flow using Equation (4.6)

These assumptions, findings and equations will be employed in the one-dimensional, finite-volume model which will now be developed from first principle.

4.2   One-dimensional model

It was stated in Chapter 1 that a goal behind the current research question is to encourage future research. An objective therefore is to ensure that the developed model is simple and easy to understand at an undergraduate engineering level. For this reason, the one-dimensional, finite-volume model will be developed from first principle in this section. The development will progress from the three conservation laws – that of mass, momentum and energy. It will also refer to the assumptions of other authors introduced in the prior section to simplify the equations resulting from these laws. Finally, a complete one-dimensional, finite-volume model of the thermosyphon loop will be presented.

4.2.1   Conservation of mass

As is shown in Figure 4.2, each control volume has only one inlet and one outlet.
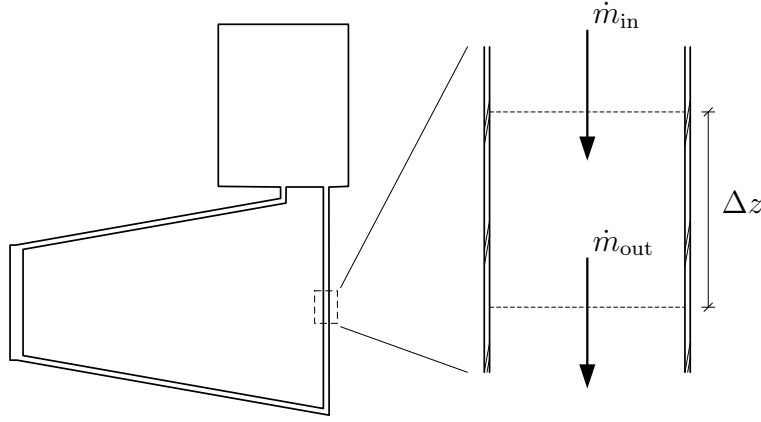
Figure 4.2: The conservation of mass on a control volume in the thermosyphon loop

Therefore, the conservation of mass through the control volume can be written as

$$\frac{\Delta m}{\Delta t} = \dot{m}_{\text{in}} - \dot{m}_{\text{out}} \tag{4.7}$$

When steady state is assumed (as discussed in the literature survey), this leads to

$$\dot{m}_{\text{in}} = \dot{m}_{\text{out}} \tag{4.8}$$

which states that the mass flow rate throughout the entire loop is constant.

4.2.2   Conservation of energy

The conservation of energy can be applied to the same control volume introduced in Figure 4.2. With reference to Figure 4.3 this is found to be

$$\frac{(\rho A \Delta z)\, \Delta h}{\Delta t} = (\dot{m}h)_{\text{in}} - (\dot{m}h)_{\text{out}} + \dot{Q}_{\text{in}} - \dot{Q}_{\text{out}} \tag{4.9}$$

Unlike with the conservation of mass, however, steady state *cannot* be assumed.

For use in the one-dimensional, finite-volume model, the explicit formulation of the transient energy equation will thus be derived.

First, Equation (4.9) is rewritten as

$$\frac{(\rho A \Delta z)\, (h_{new} - h_{old})}{\Delta t} = (\dot{m}h)_{\text{in}} - (\dot{m}h)_{\text{out}} + \dot{Q}_{\text{in}} - \dot{Q}_{\text{loss}} \tag{4.10}$$

Figure 4.3: The conservation of energy on a control volume in the thermosyphon loop

so that,

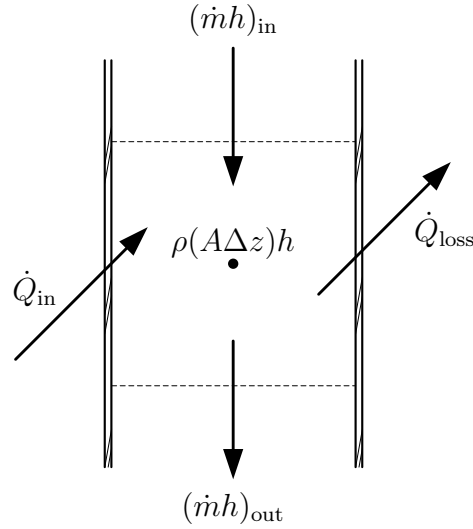$$h_{new} = \frac{\Delta t}{(\rho A \Delta z)} \left((\dot{m}h)_{\text{in}} - (\dot{m}h)_{\text{out}} + \dot{Q}_{\text{in}} - \dot{Q}_{\text{loss}} \right) + h_{old} \qquad (4.11)$$

Next, since the explicit version of this equation is to be used, all the variables on the right hand side of the equation will assume their *old* values (the values *at the previous time-step*).

$$h_{new} = \frac{\Delta t}{\rho_{old} A \Delta z} \left((\dot{m}h)_{\text{in}} - (\dot{m}h)_{\text{out}} + \dot{Q}_{\text{in}} - \dot{Q}_{\text{loss}} \right)_{old} + h_{old} \qquad (4.12)$$

This explicit formulation is written in such a way that the *new* values, in this case h_{new}, are dependent only on *old* values. The values at each time-step can thus be determined without iterations within that time-step.

Another possibility would have been to write Equation (4.12) as

$$h_{new} = \frac{\Delta t}{\rho_{new} A \Delta z} \left((\dot{m}h)_{\text{in}} - (\dot{m}h)_{\text{out}} + \dot{Q}_{\text{in}} - \dot{Q}_{\text{loss}} \right)_{new} + h_{old} \qquad (4.13)$$

This is known as the implicit formulation. In this case, all of the terms on the right hand side (except for h_{old}) depend on h_{new}. This formulation thus requires several iterations within each time-step or the usage of a matrix solver

if the equation is simple enough (as can be the case with a one-dimensional model).

From a computation time point of view, the explicit formulation is often desirable. But, it does have a disadvantage. It is not unconditionally stable. Unless the time-step is sufficiently small, the answer it gives diverges or oscillates, often severely, as time progresses (Çengel and Ghajar, 2011).

Despite this limitation, the explicit formulation will be used in the present model wherever transient equations are used. Also, for brevity, the *old* subscripts will be dropped.

The explicit Equation (4.12) can now be solved for h_{new} as long as $\dot{Q}_{\text{in}}$ and $\dot{Q}_{\text{loss}}$ are known.

Here, $\dot{Q}_{\text{in}}$ refers to the thermal energy added to the system. In the case of the experimental model (and thus the computational model that is based on it) this is a simple source of constant heat flux, applicable only to the heated area. This can later be replaced by the solar collector.

The heat lost to the environment, $\dot{Q}_{\text{loss}}$, in Equation (4.12) can be solved based on the thermal resistance diagram shown in Figure 4.4.

It is assumed heat is lost to the environment because the temperature of the water is higher than that of the ambient air. It should also be noted that the diagram does not include thermal resistances for insulation. This is since the computational model is based on the experimental set-up, which was not insulated. This should be improved in later versions of the model which will be based on the general case of a solar water heating system (which fall outside the scope of this present research).

With reference to this figure, $\dot{Q}_{\text{loss}}$ can be calculated using the following formula, as adapted from Çengel and Ghajar (2011).

$$\dot{Q}_{\text{loss}} = \frac{T_{\text{water}} - T_{\text{wall, outside}}}{\text{R}_{\text{conv, water}} + \text{R}_{\text{wall}}} = \dot{Q}_{\text{loss, conv}} + \dot{Q}_{\text{loss, rad}} \tag{4.14}$$

where, $\dot{Q}_{\text{loss, conv}}$ can also be expressed as

$$\dot{Q}_{\text{loss, conv}} = \frac{T_{\text{wall, outside}} - T_{\text{air}}}{\text{R}_{\text{conv, air}}} \tag{4.15}$$
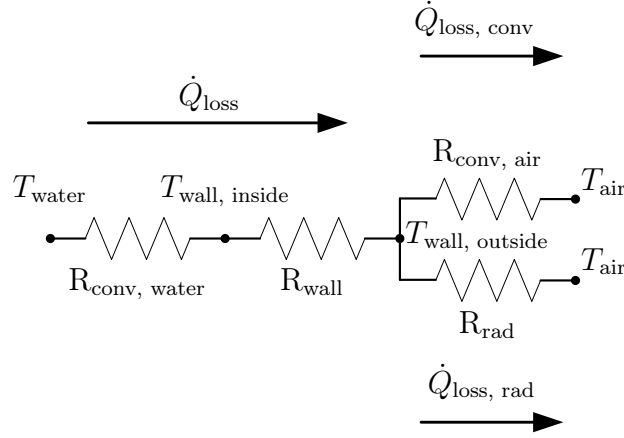
Figure 4.4: Heat transfer resistance diagram of a control volume in the thermosyphon loop

and $\dot{Q}_{\text{loss, rad}}$ as

$$\dot{Q}_{\text{loss, rad}} = \epsilon \sigma A_z (T^4_{\text{wall, outside}} - T^4_{\text{air}}) \tag{4.16}$$

Also,

$$R_{\text{wall}} = \frac{\ln(r_{\text{outside}}/r_{\text{inside}})}{2\pi \Delta z k_{\text{wall}}} \tag{4.17}$$

The two convective resistances in the above equations can be calculated as

$$R_{\text{conv}} = \frac{1}{A_z h_{\text{conv}}} \tag{4.18}$$

The convective heat transfer coefficient, h_{conv}, in this equation can be found if the Nusselt number associated with the fluid and the flow regime is known.

The Nusselt number,

$$Nu = \frac{L_c h_{\text{conv}}}{k_{\text{fluid}}} \tag{4.19}$$

is based on the thermal conductivity of the fluid, k_{fluid}, and a specific characteristic length, L_c, which should be defined for each case.

Different correlations for the Nusselt number under different conditions are available in literature. For these to be applicable in a specific case, certain assumptions are necessary and certain conditions must be met.

A simple case is the calculation of Nu_{water} (and consequently $h_{\text{conv, water}}$ and $R_{\text{conv, water}}$). It is known (Çengel and Ghajar, 2011) that the Nusselt number for forced, internal, laminar flow with a constant surface temperature,

$$\mathrm{Nu_D} = \frac{Dh_{\mathrm{conv}}}{k} = 3{,}66 \tag{4.20}$$

The flow inside the tubes in the present model is laminar and for the purpose of the above equation, can be considered as forced. This is due to the fact that it is not the heat lost to (or gained from) the environment that drives the flow, but the thermosyphon effect which is calculated using the separate momentum equation.

If the assumption is thus made, for the sake of simplicity, that the wall temperature throughout most of the loop is constant (which is true for all the sections but the heater itself), Equation (4.20) can be used to calculate $\mathrm{Nu_{D,\,water}}$.

The convective heat transfer coefficient on the outside of the tube, $h_{\mathrm{conv,\,air}}$ is based on natural convection and requires some more work.

Firstly, the Prandtl number,
$$\mathrm{Pr} = \frac{c_p \mu}{k} \tag{4.21}$$

the Grashof number,
$$\mathrm{Gr} = \frac{g\beta\Delta T L_c^3}{\left(\frac{\mu}{\rho}\right)^2} \tag{4.22}$$

and the Rayleigh number,
$$\mathrm{Ra} = \mathrm{Gr}\ \mathrm{Pr} \tag{4.23}$$

are introduced. These are non-dimensional numbers commonly associated with natural convective flows. In these flows, which specifically occur at solid surfaces, the flow is driven by the temperature difference between the surface and the fluid, ΔT.

According to work done by Ostrach (1952) and Le Fevre (1956) – as cited and recommended by Popiel (2008) – the local Nusselt number for natural convective flow from a vertical plate is

$$\mathrm{Nu}_{x-\mathrm{FP}} = (\mathrm{Gr}_x)^{1/4} \frac{0{,}75\mathrm{Pr}^{1/2}}{\left[4\left(0{,}609 + 1{,}221\mathrm{Pr}^{1/2} + 1{,}238\mathrm{Pr}\right)\right]^{1/4}} \tag{4.24}$$

In the above equation, the characteristic length (to be used in the Grashof and Nusselt numbers) is the local height of the vertical plate, measured from its bottom most point. It is valid for all Prandtl numbers.

This correlation can also be used on tubes if the diameter is sufficiently large as compared to the height. However, in the present case the tubes are to be considered slender, in that they are much longer than they are thick.

For Equation (4.24) to be valid, it thus has to be adjusted to account for the effect of the curvature of the tube. This can be done using correlations developed by Popiel (2008) from the numerical data of Cebeci (1974). The correcting correlations vary with Prandtl numbers.

For air at the expected temperatures of the current computational model,

$$\frac{\mathrm{Nu}_x}{\mathrm{Nu}_{x-\mathrm{FP}}} = 1 + 0{,}400 \left[32^{0{,}5} \left(\mathrm{Gr}_x\right)^{-0{,}25} \left(\frac{x}{D}\right) \right]^{0{,}886} \tag{4.25}$$

These equations are only valid for vertical tubes, however. To calculate the Nusselt numbers for inclined sections of the thermosyphon loop, a correlation developed by Rani *et al.* (2014) is used. According to his work, the average Nusselt number for an inclined slender cylinder is,

$$\mathrm{Nu} = \left\{ 0{,}54 + 0{,}39 \left(\frac{\mathrm{Pr}\ \mathrm{Gr}}{\left[1 + (0{,}559/\mathrm{Pr})^{9/16}\right]^{16/9}} \right)^{0{,}168} \right\}^2 \tag{4.26}$$

where the characteristic length is defined as

$$L_c = \left(\frac{LD}{(L/D)\cos\theta + (D/L)\sin\theta} \right)^{1/2} \tag{4.27}$$

With these Nusselt numbers, for both vertical and inclined tubes known, the convective heat transfer coefficient on the outside of the tube can also be calculated. With that established, the heat lost to the environment, $\dot{Q}_{\mathrm{loss}}$, can be found and Equation (4.12) can be solved for h_{new} and that used to find the new temperatures.

4.2.3 Conservation of momentum

The conservation of linear momentum can be expressed as

$$\frac{\Delta mv}{\Delta t} = (\dot{m}v)_{\mathrm{in}} - (\dot{m}v)_{\mathrm{out}} + \sum F \tag{4.28}$$

When this is applied to the control volume depicted in Figure 4.5 (which is the same volume introduced in Figure 4.2), the sum of the forces acting in the flow direction becomes

$$\sum F = P_{\text{in}} A_{\text{in}} + \rho g(A \, \Delta z) - P_{\text{out}} A_{\text{out}} - \tau A_{\text{z}} \tag{4.29}$$

The $\rho g(A \, \Delta z)$ term above is positive because gravity is acting in the direction of flow in Figure 4.5. It becomes negative if gravity opposes flow.
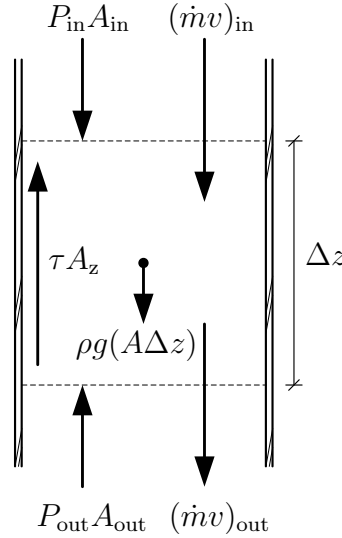
Figure 4.5: The conservation of momentum on a control volume in the thermosyphon loop

Equations (4.28) and (4.29) can be combined to yield

$$\frac{\Delta mv}{\Delta t} = (\dot{m}v)_{\text{in}} - (\dot{m}v)_{\text{out}} + P_{\text{in}} A_{\text{in}} + \rho g(A \, \Delta z) - P_{\text{out}} A_{\text{out}} - \tau A_{\text{z}} \tag{4.30}$$

In the literature surveyed, this equation was summed around the entire piping-system–storage-tank loop (ABCDA in Figure 4.1). In other word, the thermosyphon loop (ABCD in Figure 4.1) and tank (DA in Figure 4.1) are not treated separately. However, one of the objectives of the present research is to produce a complete model that consists of separate *modules* for separate components to ensure that the model is easy to expand.

In addition to modular development being a stated objective, it is also a requirement of the chosen verification technique of unit testing.

Therefore, the method found in literature has to be adjusted. For the present model, Equation (4.30) will be summed only around the piping-system loop (ABCD in Figure 4.1). It is thus summed from the *inlet* of the thermosyphon loop (which is the outlet of the tank) to the *outlet* of the thermosyphon loop (which is the central inlet to the tank).

This summation produces

$$\sum \frac{\Delta mv}{\Delta t} = \sum \rho g A \, \Delta z - \sum \tau A_{\mathrm{z}} + (\dot{m}v + PA)_{\mathrm{inlet}} - (\dot{m}v + PA)_{\mathrm{outlet}} \quad (4.31)$$

This simplification occurs since, except for at the inlet and outlet, all of the $P_{\mathrm{in's}}$, $P_{\mathrm{out's}}$, $(\dot{m}v)_{\mathrm{in's}}$ and $(\dot{m}v)_{\mathrm{out's}}$ cancel out when summing around the loop.

The equation above is applicable to any thermosyphon loop of any geometry. Because the present computational model is to be based on the experimental set-up, however, it is known that $A = \pi r^2$ and $A_{\mathrm{z}} = \pi \, 2r \, \Delta z$, so that

$$\frac{A_{\mathrm{z}}}{A} = \frac{\pi \, 2r \, \Delta z}{\pi r^2} = \frac{2 \, \Delta z}{r} \quad (4.32)$$

By further noting that $\dot{m} = \rho v A$, Equation (4.31) can be divided by A to yield

$$\sum \frac{\Delta mv}{A \Delta t} = \sum \rho g \, \Delta z - \sum \tau \left(\frac{2 \, \Delta z}{r} \right) + \left(\rho v^2 + P \right)_{\mathrm{inlet}} - \left(\rho v^2 + P \right)_{\mathrm{outlet}} \quad (4.33)$$

Equation (4.33) now has the units of Pascal. To better illustrate this, it can be rewritten as

$$\sum \frac{\Delta mv}{A \Delta t} = \Delta \mathrm{P}_{th} - \Delta \mathrm{P}_f + \left(\rho v^2 + P \right)_{\mathrm{inlet}} - \left(\rho v^2 + P \right)_{\mathrm{outlet}} \quad (4.34)$$

where

$$\Delta \mathrm{P}_{th} = \sum \rho g \, \Delta z \quad (4.35)$$

is the driving pressure due to the thermosyphon effect and

$$\Delta \mathrm{P}_f = \sum \tau \left(\frac{2 \, \Delta z}{r} \right) \quad (4.36)$$

is the pressure drop due to friction.

This pressure drop can be calculated by taking the shear stress, τ, to be

$$\tau = \frac{1}{2}C_f \rho v^2 \tag{4.37}$$

where C_f is the Fanning friction factor. It is known that, for laminar flow, $C_f = \frac{16}{\mathrm{Re_D}}$ (Çengel and Cimbala, 2010), so that

$$
\begin{aligned}
\Delta \mathrm{P}_f &= \sum \tau \frac{2}{r}\,\Delta z \\
&= \sum \left(\frac{1}{2}\left[\frac{16}{\mathrm{Re_D}}\right]\rho v^2\right)\frac{2}{r}\,\Delta z \\
&= \sum \frac{16}{\mathrm{Re_D}}\frac{\rho v^2}{r}\,\Delta z \\
&= \sum \left(\frac{64}{\mathrm{Re_D}}\frac{1}{2r}\right)\frac{\rho v^2}{2}\,\Delta z
\end{aligned}
\tag{4.38}
$$

However, $\Delta \mathrm{P}_f$, above includes only the effect of major losses because of wall friction. It omits the minor losses (due to bends and contractions, for example). These minor losses can easily be taken into account by using published loss coefficients, which are defined as

$$K_{\mathrm{L}} = \frac{\Delta \mathrm{P_m}}{\rho v^2/2} \tag{4.39}$$

where $\Delta \mathrm{P_m}$ refers to the pressure drop due to minor losses (Çengel and Cimbala, 2010). This can be added to the pressure drop due to friction to yield the total pressure drop due to major and minor losses,

$$\Delta \mathrm{P}_l = \sum \left(\frac{64}{\mathrm{Re_D}}\frac{1}{2r} + \frac{K_{\mathrm{L}}}{\Delta z}\right)\frac{\rho v^2}{2}\,\Delta z \tag{4.40}$$

This total pressure drop can then be used in Equation (4.34) instead of the pressure drop due to friction.

Another simplification to Equation (4.34) involves defining the pressure drop due to the effect of the inlet and outlet conditions as

$$
\begin{aligned}
\Delta \mathrm{P}_{\text{outlet-inlet}} &= \left(\rho v^2 + P\right)_{\text{outlet}} - \left(\rho v^2 + P\right)_{\text{inlet}} \\
&= P_{\text{outlet}} - P_{\text{inlet}} + \left(\rho v^2\right)_{\text{outlet}} - \left(\rho v^2\right)_{\text{inlet}}
\end{aligned}
\tag{4.41}
$$

Since this computational model is based on the experimental set-up, it is known that $A_{\text{inlet}} = A_{\text{outlet}}$. Also, from the conservation of mass, $\dot{m}_{\text{inlet}} = \dot{m}_{\text{outlet}}$. Therefore, and since $v = \frac{\dot{m}}{\rho A}$,

$$
\begin{aligned}
\left(\rho v^2\right)_{\text{outlet}} - \left(\rho v^2\right)_{\text{inlet}} &= \left(\rho \left[\frac{\dot{m}}{\rho A}\right]^2\right)_{\text{outlet}} - \left(\rho \left[\frac{\dot{m}}{\rho A}\right]^2\right)_{\text{inlet}} \\
&= \left(\frac{\dot{m}}{A}\right)^2 \left(\left[\frac{1}{\rho}\right]_{\text{outlet}} - \left[\frac{1}{\rho}\right]_{\text{inlet}}\right)
\end{aligned}
\tag{4.42}
$$

Finally, the transient term from Equation (4.34) can also be further simplified:

$$
\begin{aligned}
\sum \frac{\Delta m v}{A \Delta t} &= \sum \frac{(mv)_{new} - (mv)_{old}}{A \Delta t} \\
&= \sum \frac{((\rho A \Delta z)\, v)_{new} - ((\rho A \Delta z)\, v)_{old}}{A \Delta t} \\
&= \sum \frac{\Delta z}{\Delta t} \left((\rho v)_{new} - (\rho v)_{old}\right) \\
&= \sum \frac{\Delta z}{\Delta t} \left(\left(\rho \left(\frac{\dot{m}}{\rho A}\right)\right)_{new} - \left(\rho \left(\frac{\dot{m}}{\rho A}\right)\right)_{old}\right) \\
&= \sum \frac{\Delta z}{A \Delta t} \left(\dot{m}_{new} - \dot{m}_{old}\right) \\
&= \frac{\sum \Delta z}{A \Delta t} \left(\dot{m}_{new} - \dot{m}_{old}\right)
\end{aligned}
\tag{4.43}
$$

After all of these alterations, Equation (4.34) becomes

$$
\frac{\sum \Delta z}{A \Delta t} \left(\dot{m}_{new} - \dot{m}_{old}\right) = \Delta P_{th} - \Delta P_l - \Delta P_{\text{outlet-inlet}}
\tag{4.44}
$$

where,

$$
\begin{aligned}
\Delta P_{th} &= \sum \rho g\, \Delta z \\
\Delta P_l &= \sum \left(\frac{64}{\text{Re}_D} \frac{1}{2r} + \frac{K_L}{\Delta z}\right) \frac{\rho v^2}{2}\, \Delta z \\
\Delta P_{\text{outlet-inlet}} &= P_{\text{outlet}} - P_{\text{inlet}} + \left(\frac{\dot{m}}{A}\right)^2 \left(\left[\frac{1}{\rho}\right]_{\text{outlet}} - \left[\frac{1}{\rho}\right]_{\text{inlet}}\right)
\end{aligned}
\tag{4.45}
$$

This equation can be solved for $\dot{m}$ if the temperature field is known. It will now be further manipulated to investigate different possible cases of the solution. These cases are compared numerically in the validation and discussion section.

4.2.4   Conservation of momentum: transient

A first possible case is to use Equation (4.44) just as it is: in its transient form. It can then be solved for $\dot{m}_{new}$ at each time-step, yielding

$$\dot{m}_{new} = \frac{A\Delta t}{\sum \Delta z} \left(\Delta \mathrm{P}_{th} - \Delta \mathrm{P}_{l} - \Delta \mathrm{P}_{\text{outlet-inlet}} \right)_{old} + \dot{m}_{old} \qquad (4.46)$$

Note, that the equation above is in the explicit formulation.

4.2.5   Conservation of momentum: steady state

Another possibility is to assume quasi-steady state, as was done for the mass equation. This means that the momentum equation is assumed to be at steady state, at each time-step. This steady state equation is then solved for $\dot{m}$ at each time-step, after the new temperature field is calculated for that time-step using the transient energy equation.

If steady state is assumed, Equation (4.44) becomes

$$0 = \Delta \mathrm{P}_{th} - \Delta \mathrm{P}_{l} - \Delta \mathrm{P}_{\text{outlet-inlet}} \qquad (4.47)$$

so that

$$\left\{ \sum \rho g \, \Delta z \right\} = \quad \left\{ \sum \left(\frac{64}{\mathrm{Re_D}} \frac{1}{2r} + \frac{K_{\mathrm{L}}}{\Delta z} \right) \frac{\rho}{2} \left(\frac{\dot{m}}{A\rho} \right)^2 \Delta z \right\}$$
$$+ \left\{ P_{\text{outlet}} - P_{\text{inlet}} + \left(\frac{\dot{m}}{A} \right)^2 \left(\left[\frac{1}{\rho} \right]_{\text{outlet}} - \left[\frac{1}{\rho} \right]_{\text{inlet}} \right) \right\} \qquad (4.48)$$

This can be further reduced to

$$\sum \rho g \, \Delta z + P_{\text{inlet}} - P_{\text{outlet}} = \left(\frac{\dot{m}}{A} \right)^2 \Bigg\{ \quad \left[\sum \left(\frac{64}{\mathrm{Re_D}} \frac{1}{2r} + \frac{K_{\mathrm{L}}}{\Delta z} \right) \frac{1}{2\rho} \Delta z \right]$$
$$+ \left(\left[\frac{1}{\rho} \right]_{\text{outlet}} - \left[\frac{1}{\rho} \right]_{\text{inlet}} \right) \quad \Bigg\}$$
$$(4.49)$$

Finally, $\dot{m}$ can then be solved as

$$\dot{m}^2 = A^2 \frac{\sum \rho g \Delta z + P_{\text{inlet}} - P_{\text{outlet}}}{\sum \left(\frac{64}{\text{Re}_{\text{D}}} \frac{1}{2r} M + \frac{K_{\text{L}}}{\Delta z} \right) \frac{1}{2\rho} \Delta z + \left(\frac{1}{\rho} \right)_{\text{outlet}} - \left(\frac{1}{\rho} \right)_{\text{inlet}}} \tag{4.50}$$

The effect that using these two different forms of the momentum equation has on the model will be explored in the section: validation and discussion.

4.2.6 Conservation of momentum: comparison to literature

Before the numerical data is introduced, however, the momentum equation of the current computational model, Equation (4.44), will first be compared with the momentum equation introduced as part of the literature survey, Equation (4.1). It will also be shown that Equation (4.1), which is used by all the surveyed models, can be derived as a restricted case of the more generally applicable Equation (4.44).

Firstly, according to the framework from the surveyed literature, steady state is assumed for the momentum equation. In the current model, both the steady state and transient momentum equations can be used. For the derivation of Equation (4.1), the steady state Equation (4.47) is thus used.

Secondly, the models from literature all find the momentum equation by summing Equation (4.28) around a closed loop. In contrast, Equation (4.47) allows for the calculation of mass flow rate around an open loop, subject to knowing the entry and exit conditions. This restriction from literature can be incorporated into Equation (4.47) by assuming that $\Delta P_{\text{outlet-inlet}}$. This yields,

$$0 = \Delta P_{th} - \Delta P_l - 0 \tag{4.51}$$

so that,

$$\Delta P_{th} = \Delta P_l \tag{4.52}$$

Thirdly, the models from literature calculate the mass flow rate from an equation defined in terms of head in meters, not pressure difference in terms of Pascal. To incorporate this into Equation (4.52), it must be divided by $\bar{\rho}g$, resulting in

$$h_{th} = h_l \tag{4.53}$$

This division (which influences the calculation of $\dot{m}$) introduces an unnecessary, albeit very small, error since it is based on the assumption that the difference between the local density anywhere in the loop, ρ and the average density, $\bar{\rho}$ is negligible.

Finally, one of the models surveyed from literature suggest an addition can be made to the current computational model. This is in contrast to the restrictions thus far required to make the current model conform to those in literature. This addition is found in the work of Morrison and Ranatunga (1980a,b). They suggest that a correction factor, M, be included in the calculation of the total head losses, h_l. This is to account for the flow in some regions of the tube that is still developing, and not fully developed laminar, as is assumed.

This can be incorporated into the present model by changing the definition of the total pressure drop due to major and minor losses as follows

$$\Delta P_l = \sum \left(\frac{64}{Re_D} M \frac{1}{2r} + \frac{K_L}{\Delta z} \right) \frac{\rho v^2}{2} \, \Delta z \tag{4.54}$$

where,

$$M = 1.0 + \frac{0{,}038}{(\Delta z / D \ Re_D)^{0{,}96}} \tag{4.55}$$

The effect of this inclusion of M on the computational model is also discussed in the next section.

4.3   Validation and discussion

The model previously derived will here be validated. As was described in Chapter 2, this will be done by graphical comparison and subjective validation.

Towards this end, several experiments were conducted using the set-up described in Chapter 3.

The set-up was filled with cold water and the heater turned on at time = zero seconds. Temperature and velocity measurements were then taken at 30 s intervals. This was done at two different heater settings.

To ensure repeatability, the experiment was run three different times at each heater setting, with very little discrepancy between the runs.

Figures 4.6 and 4.7 show the comparison between the measured and calculated outlet temperatures for the two heater settings.
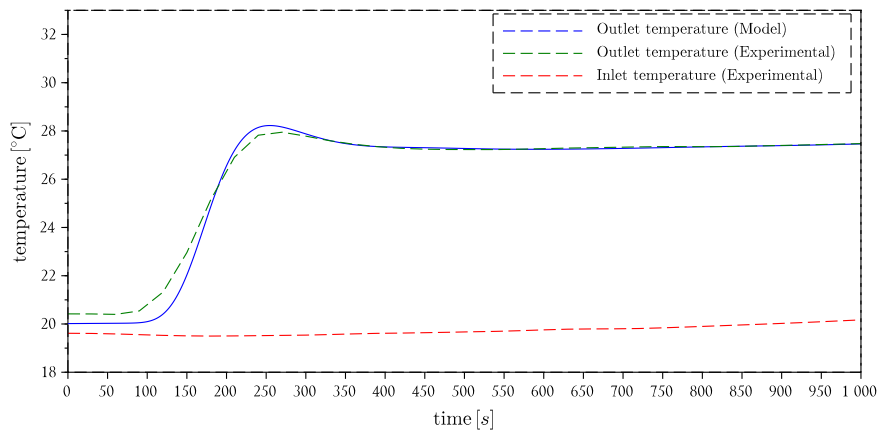
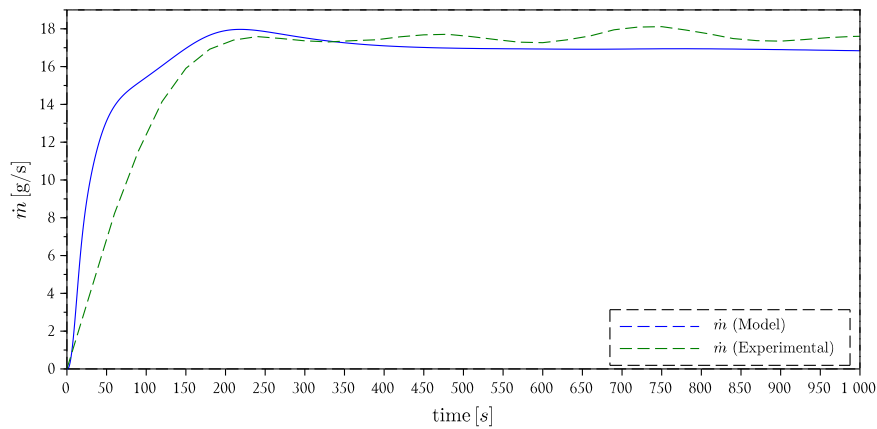**Figure 4.6:** Temperature comparison plot for the 550 W experiment
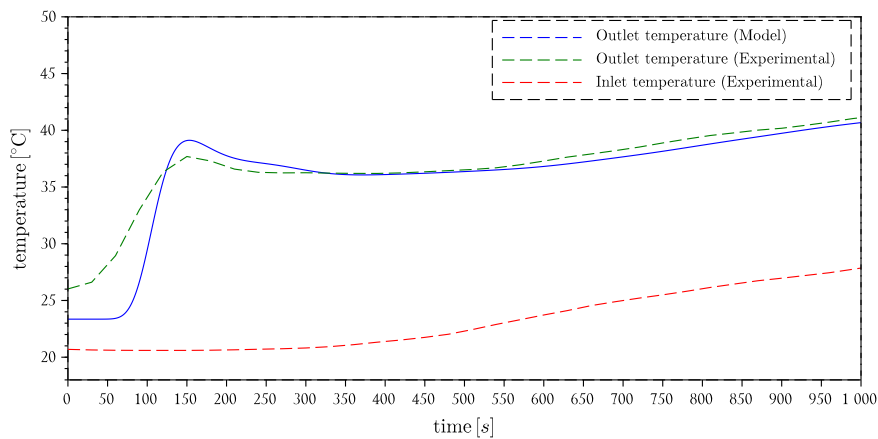
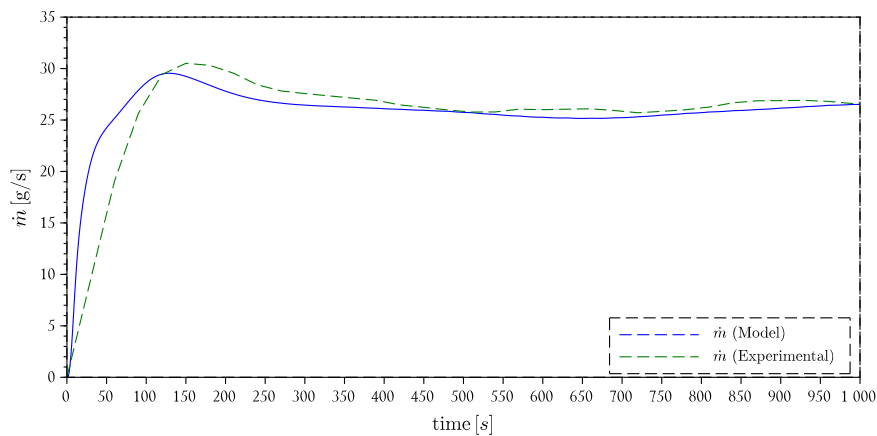**Figure 4.7:** Temperature comparison plot for the 1 500 W experiment

In both cases, the model uses the experimental inlet temperature as a boundary condition. The thermosyphon loop model could have used the output of the plume model (still to be discussed), but this would have violated the chosen verification strategy of unit testing.

It can be seen from the two figures that the model very closely relates to the measured data. This is especially true at later time-steps.

Figures 4.8 and 4.9 show the mass flow rate comparisons between the calculated and measured data at the two heater settings.

Figure 4.8: Mass flow rate comparison plot for the 550 W experiment

Figure 4.9: Mass flow rate comparison plot for the 1 500 W experiment

It is once more seen that the model closely compares with the experimental data.

It should be noted, however, that the model does a much better job capturing steady state flow than it does transients. This poor transient response is

especially evident for the large step change in energy input into the system at $t = 0$.

That does not mean the model is entirely incapable of dealing with changing conditions, though. It can be seen from the 1 500 W experiment that as the input temperature gradually rises, so does the outlet temperature. This occurrence is actually captured in the model, as Figure 4.7 shows.

It can therefore be concluded that the model does very well in predicting steady state flow, as well as gradual changes. Since these are the conditions most often to be encountered in an actual solar water heating system, the model can thus be deemed valid.

It was in an attempt to correct this poor transient response that the transient momentum equation was used.

In addition to proving the model's validity, a number of other observations can also be made from the experimental data.

4.3.1   Velocity measurement

It can be noted from Figure 4.8 that there are small oscillations in the measured mass flow rate during the "steady state" portion of the experiment. This could indicate a transient in the flow that the model completely fails to capture.

However, a more likely explanation is that this is due to a measurement error in the fluid velocity. Evidence supporting this explanation can be found in Figures 4.10 and 4.11.

These figures plot the mass flow rates measured during different runs of the experiments. It can be seen that the oscillating flow rate is not a recurring phenomenon. If the average of flow rates from each run were to be taken, these oscillations would be lost.

A reason for this error can be seen in Figure 4.12. This shows the die, that was used to measure the speed of the flow, traveling along a section of the tube.

The figure shows that the die is eventually swept to the centre of the tube. (It is initially forced to the bottom, since it is injected from the top.) It was therefore assumed that the velocity measured by timing the flow of the die is
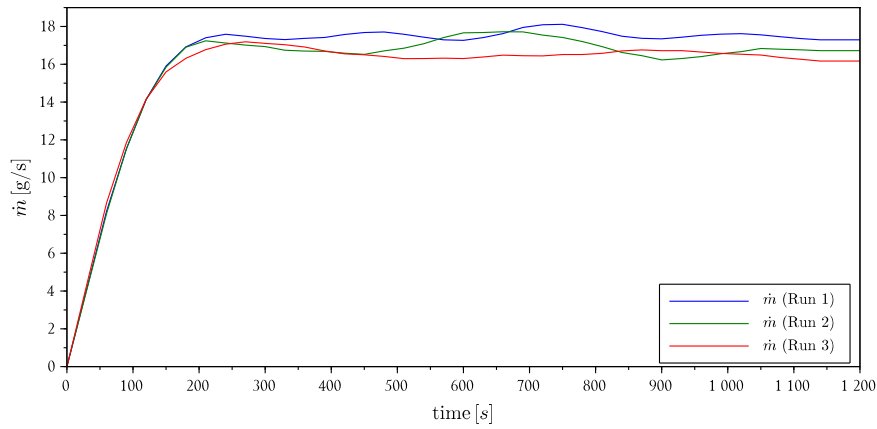
Figure 4.10: Mass flow rates measured during different runs of the 550 W experiment
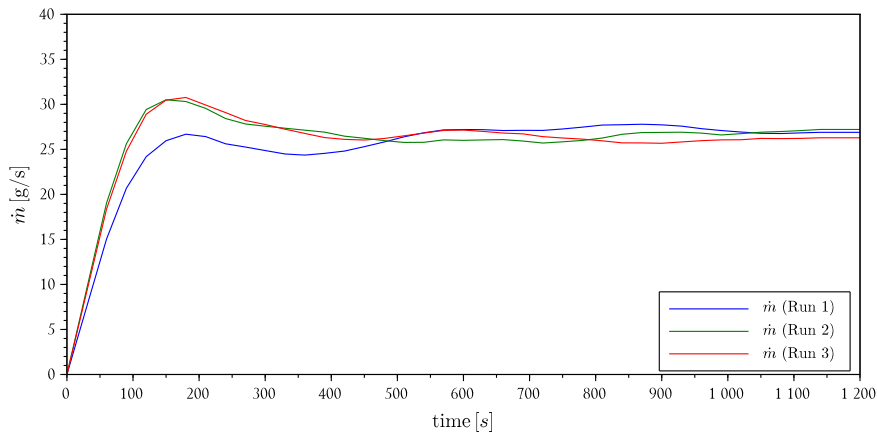
Figure 4.11: Mass flow rates measured during different runs of the 1 500 W experiment

the centreline velocity of the tube. Further scrutiny of Figure 4.12 does however reveal that this is not always the case. Deviations of the die stream from the exact centre of the tube causes an error in the mass flow rate calculated and this could be the oscillations seen in Figure 4.8.

4.3.2 Variations in the momentum equation

As was discussed during the derivation of the momentum equation, four instances thereof was tested. These are the transient and steady state equations,

Figure 4.12: Die traveling along the top tube in the experimental set-up

as well as both equations including the effect of Morrison and Ranatunga's correction factor, M.

Figure 4.13 shows a comparison of the mass flow rates found when steady state is assumed versus when it is not. This shows that this specific assumption
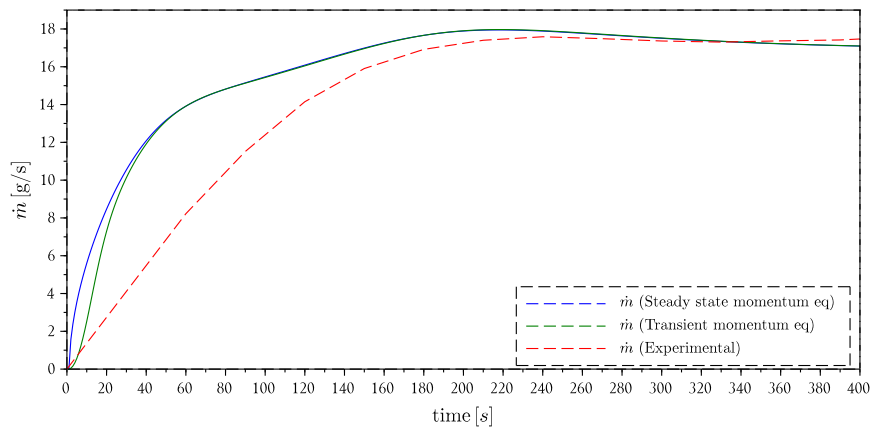
Figure 4.13: Difference between the transient and steady state momentum equations on the mass flow rate of the 550W experiment

has only a very small effect on the model. This is further evidenced in the

maximum 0,06 °C difference in the outlet temperature the two versions of the momentum equation results in.

Furthermore, the effect of including Morrison and Ranatunga's M term was even smaller.

4.3.3   Heat transfer

It was, unfortunately, not possible to individually test the heat transfer assumptions made. These assumptions can thus only be assumed valid because they conform to the conditions stated in literature as their requirements.

Despite that limitation, the overall heat loss to the environment can be compared to experimental data.

From the general transient energy equation applicable to each node, Equation (4.9) it can be seen that

$$0 = (\dot{m}h)_{\text{in}} - (\dot{m}h)_{\text{out}} + \dot{Q}_{\text{in}} - \dot{Q}_{\text{out}} \tag{4.56}$$

if an important assumptions is made. This assumption is that steady state exists and is valid for the 550 W experiment when the time, t, exceeds 400 s.

Under this condition, Equation (4.56) can be summed around the loop to yield

$$\dot{Q}_{\text{out, total}} = (\dot{m}h)_{\text{inlet}} - (\dot{m}h)_{\text{outlet}} + \dot{Q}_{\text{in, total}} \tag{4.57}$$

which enables the calculation of the "experimental" $\dot{Q}_{\text{out, total}}$. Figure 4.14 compares this value to the total heat lost to the environment as calculated by the model.

It should be noted that the oscillating value of the "experimental" heat loss can be attributed to the velocity measurement error previously discussed. It can then be seen that the modelled heat loss does follow the average "experimental" heat loss. Although this is a promising result, it is not conclusive, since the uncertainty involved in the "experimental" value is so large. However, considering the overall performance of the model in predicting mass flow rate and temperature, the model is still deemed valid.
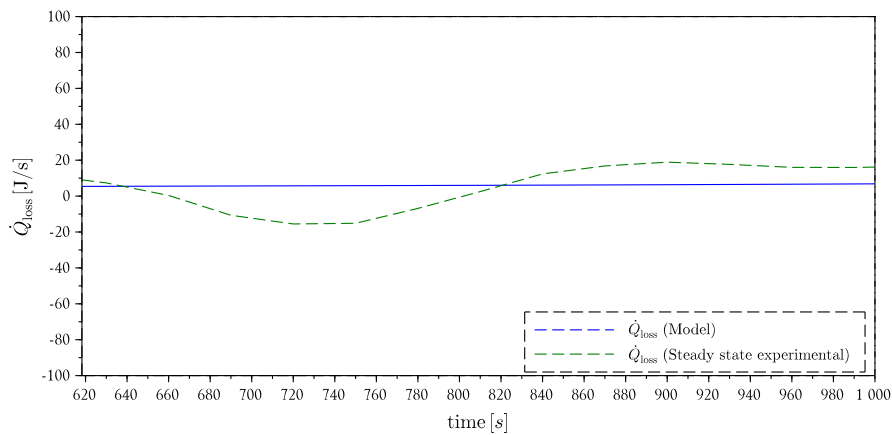
Figure 4.14: Heat loss to the environment during the steady state portion of the 550 W experiment

4.3.4 Grid and time-step analysis

With validity established, one of the steps that still has to be taken to verify that the computer model does indeed conform to the mathematics it is built on, is grid and time-step analysis. In this verification process, the model is tested at several different time-steps and using different amounts of nodes.

This was done for the present model using the input data of the 550 W experiment.

Figure 4.15 shows a plot comparing the outlet temperatures at 7 different time-step sizes. In this test, 41 nodes were used. This is the smallest number of nodes that still captures the physical details of the experimental set-up.

It can be seen from Figure 4.15 that the model's predictions are much closer together at finer time-steps than larger ones. This suggests that at some point, time-step independence is reached.

It is also apparent from the figure that at some point, the time-steps can become too large and the model's predictions are completely wrong. (For this test a time-step of 4 s resulted in such a sudden departure from the predictions at other time-steps.) This is in accordance with the stated limitation of the explicit scheme: it requires a fine enough time-step to be stable.

Except for this unstable case, it is further seen that the time-step size only
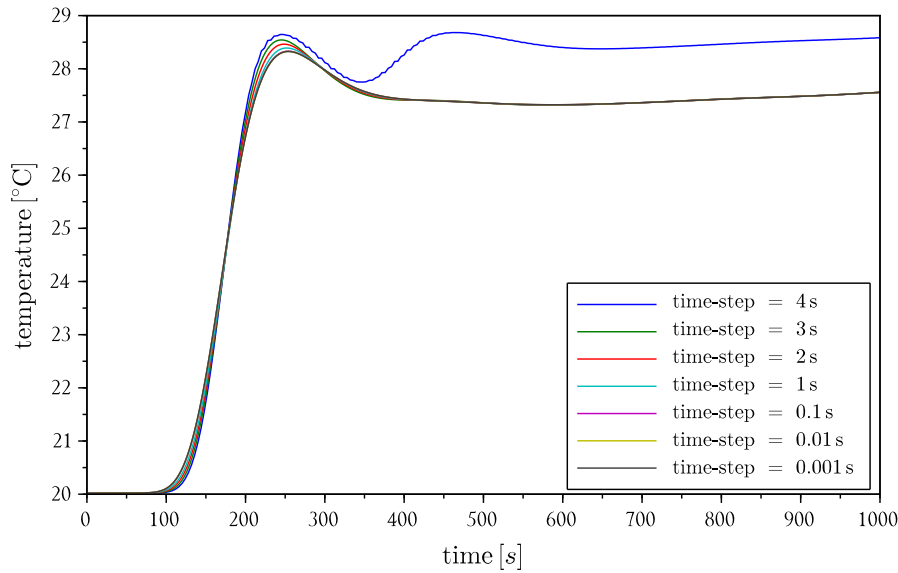
Figure 4.15: Outlet temperatures for a grid of 41 nodes at different time-steps

affects the transient behaviour of the system. At steady state, the size of the time-step has very little effect, as can be expected.

The instability of the model at too large a time-step (4 s in the present test) is clearly illustrated in Figure 4.16, which plots the mass flow rate (still using 41 nodes) at different time-steps.

By performing the above analysis for different grid sizes (82, 205 and 410 nodes were tested), Figure 4.17 was constructed. This shows the largest time-step at which time-step independence can be assumed, for different grid sizes. The data in the graph is based on the assumption that the model becomes time-step independent when further decreasing the time-step has less than a 0,1 °C impact on the outlet temperature.
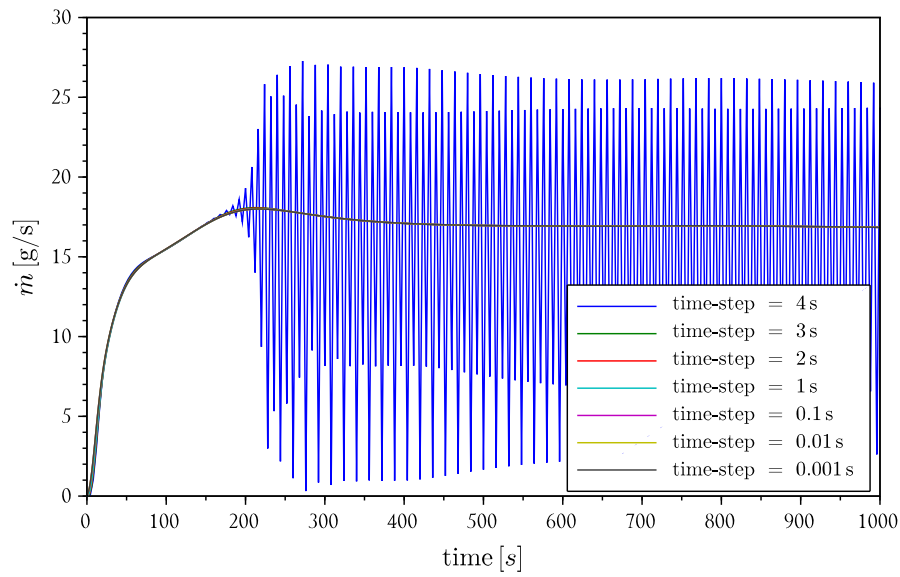
Figure 4.16: Mass flow rates for a grid of 41 nodes at different time-steps
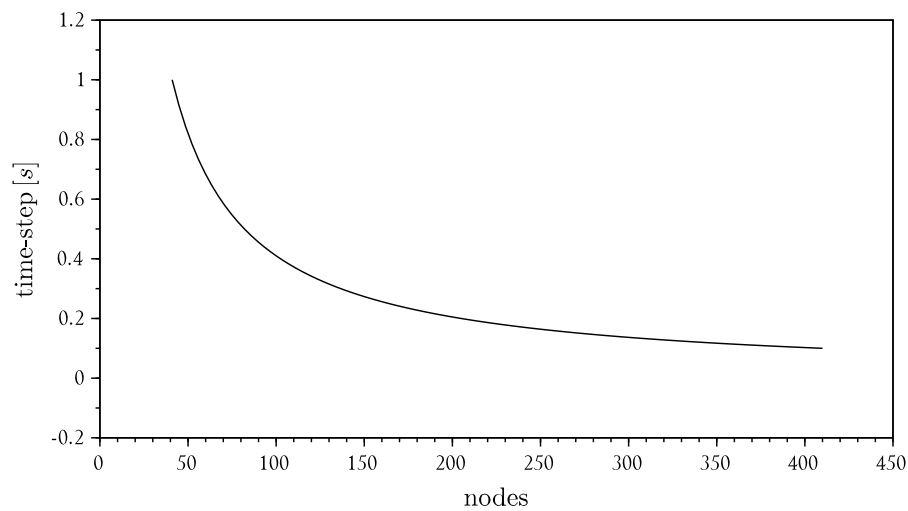
Figure 4.17: Largest time-step at which time-step independence is achieved

Chapter 5

Plume model

5.1 Literature survey

The thermosyphon loop models previously discussed, all employ one of three tank models, according to Morrison and Tran (1984)...

- Fully mixed: Incident energy is mixed throughout the tank and the average temperature taken.

- Fully stratified: New fluid enters and moves to the appropriate level (depending on its temperature) without mixing at all. (This model overestimates performance).

- Combination: New fluid still moves to a layer appropriate to its temperature, but fully mixes with all layers between the incident and the final one.

These tank mixing assumptions result in the mixing mechanisms not being modelled. In many practical implementations this is important. For the present model to be as adaptable as possible, neither of these three tank models can thus be used. For this reason, an entirely different, but applicable body of knowledge is introduced: plume formation and entrainment.

When hot fluid is injected into colder fluid, the hot fluid rises due to buoyancy forces. As it moves upward, it entrains fluid from its surrounding into itself. The radius of the rising body of warmer fluid thus increases with an increase

in height. This rising body of warmer fluid is known as a plume. Figure 5.1 shows an example of such a plume. The hot water injected into the cold tank in the figure has been mixed with die so that the plume is clearly visible.
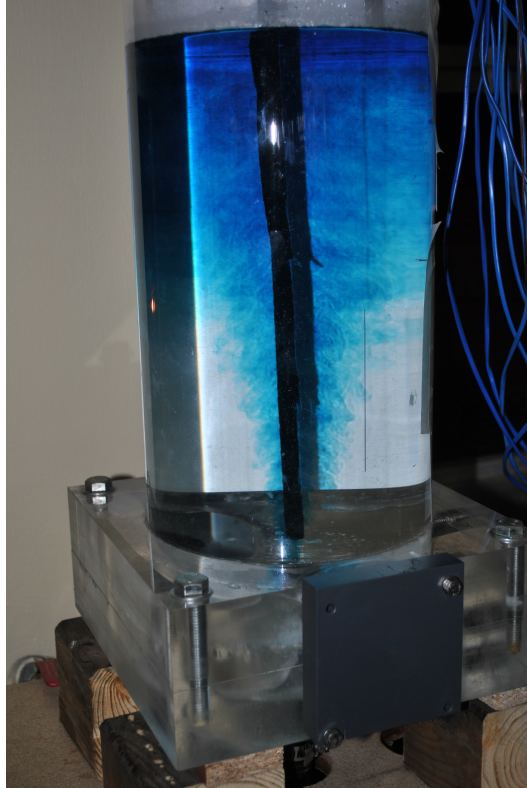
Figure 5.1: An example of a buoyant plume, rising in a tank of cold water

The present one-dimensional, finite-volume model will model the HWST as a body of water with a buoyant plume being injected into it. This section thus focusses on literature pertaining to plume theory.

Several review articles on the subject have been published, the most recent being that of Kaye (2008); Woods (2010); Hunt and van den Bremer (2011). This present review will, however, focus on the development of the theory as it pertains to the hot water storage tank of an integrated collector storage solar water heating system.

Classic plume theory is largely based on the work of Morton *et al.* (1956) and will be discussed from their paper of 1956 onwards.

Morton *et al.* (1956) simplified the governing equations of continuity, momentum and energy conservation to a set of three coupled ordinary differential equations, the first two of which are here presented.

$$\frac{\mathrm{d}}{\mathrm{d}z}\left(\rho v r^2\right) = \rho_0 \alpha v 2r \tag{5.1}$$

$$\frac{\mathrm{d}}{\mathrm{d}z}\left(\rho v^2 r^2\right) = r^2 g \left(\rho_0 - \rho\right) \tag{5.2}$$

These simplifications are based on the following assumptions

- The flow is assumed to be inviscid, an assumption supported by Hunt and van den Bremer (2011).

- The plume is assumed to be long and thin and therefore the variation of pressure with height is far greater than the variation of pressure with radius, so that the latter can be neglected. A constant (hydro-statically determined) pressure can thus be assumed for the plume and its surrounding fluid at a certain height.

- The boundary of the plume is taken to be the radius (at each height) at which the upward velocity becomes zero. The plume is thus moving within stationary fluid.

- The velocity in the plume can be taken as constant across its cross section at a certain level.

- The velocity of fluid being entrained into the plume is proportional to the upward plume velocity at that height.

The final assumption, was first proposed by Taylor (1945). According to this,

$$v_{\text{ent}} = \alpha v \tag{5.3}$$

This assumption has been challenged, defended and discussed by many authors (Turner, 1986; Hunt and Kaye, 2005; Kaye, 2008; Baines, 2014) but is widely accepted in most literature. The value of the entrainment factor, α, is usually taken to be about 0,1.

The simplified governing equations of Morton *et al.* (1956) can be solved ana-lytically, but only for constant sources of buoyancy and if the ambient fluid has a constant density. This was improved upon somewhat by Scase *et al.* (2006), allowing an analytical solution for the case where the source strength is dimin-ishing with time. The initial work of Morton *et al.* (1956) also rested upon the Boussinesq approximation, but later work (Hunt and van den Bremer, 2011) extended the theory to include the non-Boussinesq case. Unfortunately, no analytical solution exists for a plume in a stratified environment, according to Baines (2014). Such a problem needs to be solved numerically.

5.2 One-dimensional model

The assumptions introduced in the previous section will now be incorporated into a one-dimensional, finite-volume model. As was done in the case of the thermosyphon loop, this model is developed by applying the conservation equa-tions to finite control volumes within the flow domain. In keeping with the chosen validation technique, this derivation will also be based on the accepted assumptions previously introduced.

A key feature of the plume model, is that the flow domain is divided into three distinct parts, namely, the plume, the tank and above the thermocline. Figure 5.2 shows these parts and the control volumes within them.

To best describe the flow through these control volumes, the discussion will start with the conservation of linear momentum in the flow direction.

5.2.1 Conservation of momentum

It is assumed that hot water in the plume flows upwards.The only mixing between the tank and the plume volumes is as a result of entrainment as water from the tank is sucked into the plume. These flow assumptions are shown on Figure 5.3. (This figure is an enlargement of window (b) shown in Figure 5.2).

With reference to the plume control volume in Figure 5.3, the conservation of momentum for each *plume* cell can be written as

$$\frac{\Delta mv}{\Delta t} = (\dot{m}v)_{\text{in}} - (\dot{m}v)_{\text{out}} + P_{\text{in}}A - P_{\text{out}}A - \rho g(A \ \Delta z) \qquad (5.4)$$
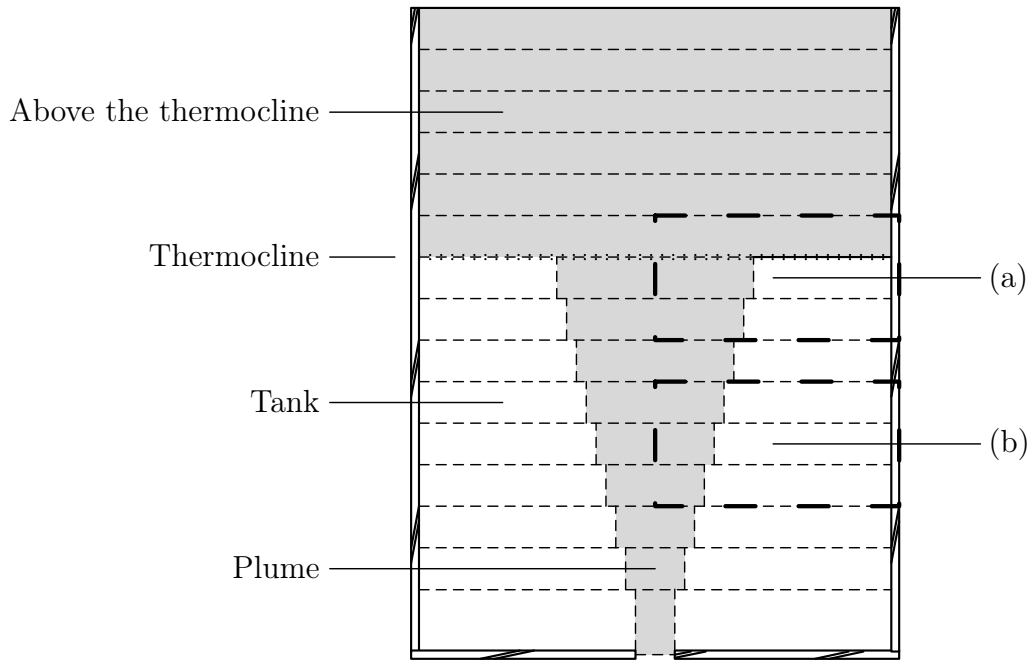
Figure 5.2: Two part plume model discretisation scheme
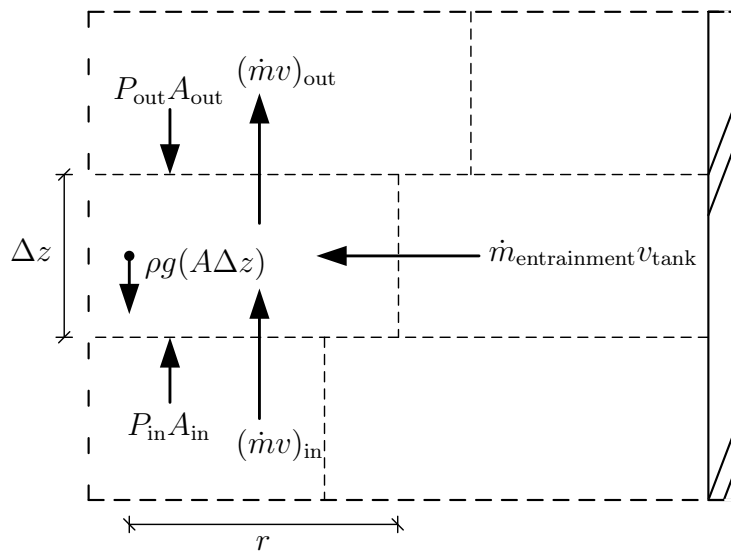
Figure 5.3: The conservation of momentum on a control volume in the buoyant plume

Note that no friction forces are present. This is because the flow is assumed to be inviscid, as discussed in the prior section. Also note that as far as conservation of momentum is concerned, v_{tank} is taken to be zero. Even though this present model treats the velocity profile across the plum as a step change

from the average plume velocity to the average tank velocity, this is not what is observed. As was discussed in the previous section, the definition of the plume boundary is the distance from the plume centre where the velocity is zero. For this reason, it is accepted that the fluid carried into the plume by entrainment carries with it negligible amounts of momentum in the z direction.

Another important assumption is that the momentum equation can be solved at steady state. This is in contrast to the momentum equation used in the thermosyphon loop model. The credibility of this assumption will be discussed along with the validating data presented in the next section.

By now assuming steady state, noting that $\dot{m} = \rho v(\pi r^2)$ and by dividing by π throughout, Equation (5.4) becomes

$$\left(\left(\rho v r^2\right) v\right)_{\text{out}} - \left(\left(\rho v r^2\right) v\right)_{\text{in}} = P_{\text{in}} r^2 - P_{\text{out}} r^2 - \rho g(r^2 \, \Delta z) \qquad (5.5)$$

This can be further simplified by assuming that the plume is long and thin. Therefore, pressure variations across the surface area of the plume are negligible compared to pressure variations along it. According to this assumption, the pressure at any point inside the plume can be taken to be the same as the pressure of the stationary fluid outside the plume at the same level. With the goal of obtaining a formula for the pressure outside the plume, a force balance is applied to an arbitrary control volume depicted in Figure 5.4. (This control volume does not represent one of the *tank* control volumes, but is merely a means of determining the pressure variation inside the plume.)

Assuming that this control volume is at the same level and of the same height as the one shown in Figure 5.3, but that no fluid is flowing through it, it's force balance yields

$$P_{\text{in}} A' = P_{\text{out}} A' + \rho_0 g(A' \, \Delta z) \qquad (5.6)$$

$$P_{\text{in}} = P_{\text{out}} + \rho_0 g \, \Delta z \qquad (5.7)$$

Substituting Equation (5.7) into Equation (5.5) and dividing throughout by Δz then yields
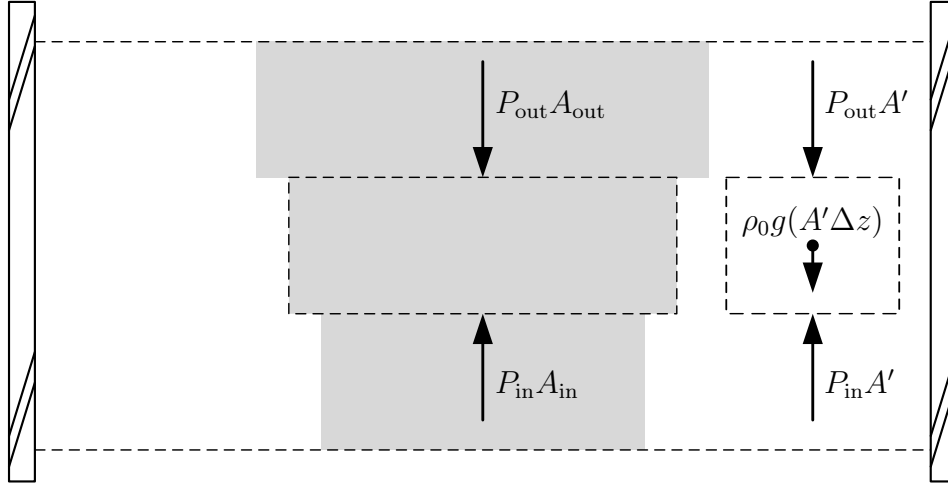
Figure 5.4: The conservation of momentum on an arbitrary control volume outside the buoyant plume

$$\frac{\left(\rho v^2 r^2\right)_{\text{out}} - \left(\rho v^2 r^2\right)_{\text{in}}}{\Delta z} = r^2 g \left(\rho_0 - \rho\right) \tag{5.8}$$

Equation (5.8) – like Equation (5.14) still to be discussed – is in the form applicable to a finite control volume and is used in the one-dimensional, finite-volume model. If the limit of this equation is taken as Δz approaches an infinitesimal size, it becomes

$$\frac{\mathrm{d}}{\mathrm{d}z}\left(\rho v^2 r^2\right) = r^2 g \left(\rho_0 - \rho\right) \tag{5.9}$$

which corresponds to Equation (5.2). It is the conservation of momentum equation developed for a plume by Morton *et al.* (1956) which was discussed in the previous section.

Focussing once more on the one-dimensional, finite-volume model, however, Equation (5.8) can be further rearranged to calculate the exit velocity of each plume section, yielding

$$v_{\text{out}} = \sqrt{\frac{r^2 g \left(\rho_0 - \rho\right) \Delta z + \left(\rho v^2 r^2\right)_{\text{in}}}{\left(\rho r^2\right)_{\text{out}}}} \tag{5.10}$$

If the inlet velocity and the temperatures inside and outside the plume are known, Equation (5.10) can be used to find the entire velocity field.

Upon closer examination, it can be seen that the sign (positive or negative) of the $r^2 g \left(\rho_0 - \rho \right) \Delta z$ (or just the $\rho_0 - \rho$) term determines whether the plume is accelerating or decelerating. At the base of the tank, the plume is much hotter than the water in the surrounding tank. Therefore, the plume density, ρ is much lower than the tank density, ρ_0. Under these conditions, the $\left(\rho_0 - \rho \right)$ term is positive and the flow is accelerating. As the plume rises, however, its temperature drops due to the entrainment of colder water from outside the plume. Meanwhile, the tank temperature higher up is warmer than that lower down (this is explained in the next subsection). Higher up the plume, the $\left(\rho_0 - \rho \right)$ term is thus smaller than at its base. At some point, as the plume rises, the plume temperature becomes lower than the tank temperature and the now negative $\left(\rho_0 - \rho \right)$ term causes the plume to slow down. Eventually its velocity is zero and the fluid that was part of the plume moves out and down into the tank.

The obviously important $\left(\rho_0 - \rho \right)$ term, or more appropriately $g \left(\rho_0 - \rho \right)$ is what is known as the buoyancy term. Apart from the initial inlet velocity, it is the only source or sink of momentum in Equation (5.10).
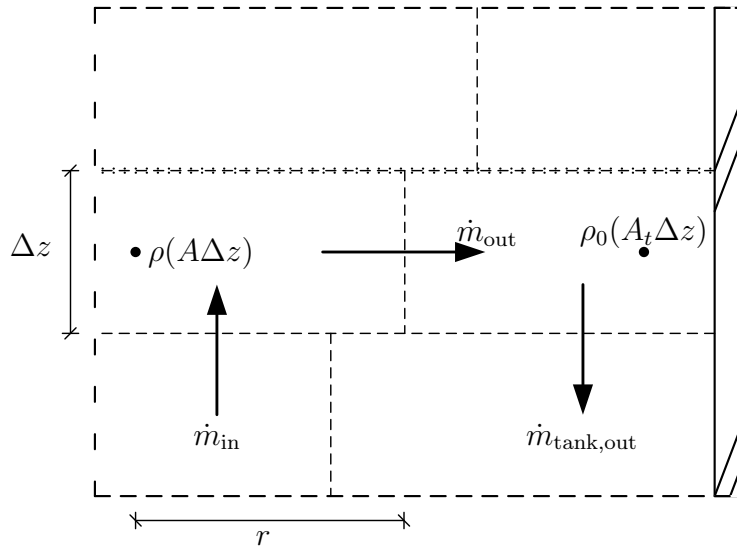
5.2.2   Conservation of mass

The outward movement of water from the plume to the tank is a complicated phenomenon that is simplified in this model by the assumption of a "hard" thermocline. Instead of allowing the plume to slow down gradually once it passes a point where the tank is hotter than the plume, the upward plume velocity is assumed to stop instantly. . . *at the thermocline.*

The thermocline in a stratified body of water usually refers to the region in which the temperature gradient is the steepest. In this present model, the thermocline refers to the separation between the moving plume and tank below, and the assumed stationary fluid above it. The height of the thermocline is the height at which the tank temperature first equals or exceeds the plume temperature.

This assumption and its implication on mass flow is depicted in Figure 5.5. (This figure is an enlargement of window (a) in Figure 5.2)

The imaginary, instant thermocline is thus treated as a hard wall. It forces all

Figure 5.5: The conservation of mass on a control volume in the buoyant plume, just below the thermocline

water that flowed into the plume volume just below it to flow sideways into the tank volume at that level. This, in turn, causes some of the water that used to be in that tank control volume to move downward. This accounts for the downward velocity accepted in all of the tank control volumes. It also explains why the tank volumes are warmer higher up the plume, since they are gradually filled with warm water that exited the plume just below the thermocline.

Figure 5.6 shows this downward flow in the tank. Depicted are adjacent plume and tank control volumes lower down the plume. This figure is thus an enlargement of window (b) in Figure 5.2.

The application of the conservation of mass principle to the *plume* control volume depicted in Figure 5.6 yields

$$\frac{\Delta m}{\Delta t} = \dot{m}_{\text{in}} - \dot{m}_{\text{out}} + \dot{m}_{\text{ent}} \tag{5.11}$$

If steady state is assumed, this becomes
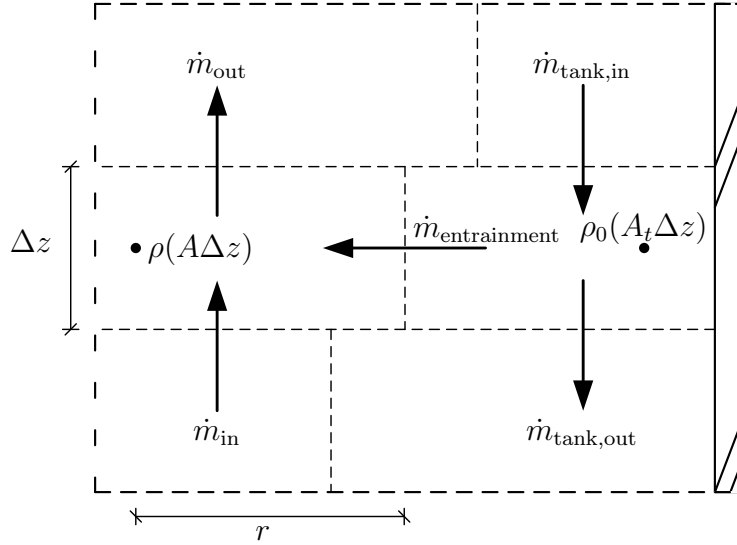
Figure 5.6: The conservation of mass on a control volume in the buoyant plume

$$\dot{m}_{\text{out}} - \dot{m}_{\text{in}} = \dot{m}_{\text{ent}}$$

$$(\rho v A)_{\text{out}} - (\rho v A)_{\text{in}} = (\rho v A)_{\text{ent}}$$

$$\left(\rho v \left(\pi r^2\right)\right)_{\text{out}} - \left(\rho v \left(\pi r^2\right)\right)_{\text{in}} = (\rho v)_{\text{ent}} \left(\pi 2 r \ \Delta z\right) \tag{5.12}$$

At this point, the important assumption that the entrainment velocity, v_{ent}, is proportional to the mean plume velocity, v, is applied. Specifically, $v_{\text{ent}} = \alpha v$. Also, the fluid entrained has the density of ρ_0, which is the density of the fluid in the tank at the same level as the control volume under consideration, but outside the plume. Equation (5.12) above thus becomes

$$\left(\rho v r^2\right)_{\text{out}} - \left(\rho v r^2\right)_{\text{in}} = \rho_0 \left(\alpha v\right) 2 r \ \Delta z \tag{5.13}$$

When this is divided by the length of the control volume in the flow direction (Δz), it yields

$$\frac{\left(\rho v r^2\right)_{\text{out}} - \left(\rho v r^2\right)_{\text{in}}}{\Delta z} = \rho_0 \alpha v 2 r \tag{5.14}$$

Equation (5.14) is in the form applicable to a finite control volume and will be used in the one-dimensional, finite-volume model. If, however, the limit of

this equation is taken as Δz approaches an infinitesimal size, Equation (5.14) becomes

$$\frac{\mathrm{d}}{\mathrm{d}z}\left(\rho v r^2\right) = \rho_0 \alpha v 2r \tag{5.15}$$

This corresponds to Equation (5.1). It is the conservation of mass equation developed for a plume by Morton *et al.* (1956) which was discussed in the previous section.

Equation (5.15) will not be used in the one-dimensional, finite-volume model, however. The equations thusfar derived from the conservation of mass on a plume volume is to be used instead to calculate the various plume radii for all the nodes at each time-step. To accomplish this, Equation (5.14) has to be rewritten as a polynomial in term of r. This is possible by noting from Figure 5.6 that $r_{\mathrm{out}} = r_{\mathrm{ent}} = r$. Equation (5.12) thus becomes

$$\left(\rho v \left(\pi r^2\right)\right)_{\mathrm{out}} - (\rho v)_{\mathrm{ent}}\left(\pi 2r\ \Delta z\right) - \dot{m}_{\mathrm{in}} = 0$$
$$(\rho v \pi)_{\mathrm{out}}\, r^2 - (\rho v 2\pi \Delta z)_{\mathrm{ent}}\, r - \dot{m}_{\mathrm{in}} = 0 \tag{5.16}$$

If the roots of this equation are found, the radius of the plume volume becomes known. Note that this formula requires the knowledge of $\dot{m}_{\mathrm{in}}$. This is similar to the equation used to calculate plume velocity, Equation (5.10). In both these cases, the mass flow rate or velocity of the inlet (to the tank, from the thermosyphon loop) must be known. From this known mass flow rate, the radius of the first plume cell can be calculated using Equation (5.16). With the radius known, the mass flow rate out of this control volume (as well as the entrainment mass flow rate) can be calculated from Equation (5.12). This newly calculated mass flow rate out of the current control volume then becomes the mass flow rate into the next control volume and the process is repeated. By so marching along the plume, all the radii and mass flow rates can be found until the thermocline is reached. At the control volume just below the thermocline, the only unknown is the mass flow rate out of the plume and into the tank control volume. This then enables the marching down the tank control volumes, calculating all tank mass flow rates as well.

This entire process requires the knowledge of the inlet conditions, as well as all the velocities along the plume. These velocities can be found using Equation (5.10). However, both this equation and Equation (5.13) assumes the knowledge of the densities within the plume and tank control volumes at the time-spans in question. The calculation thereof will now be considered.

5.2.3   Conservation of energy

In a manner similar to the prior two conservation laws, the conservation of energy can be applied to the plume control volume depicted in Figure 5.7. This results in

$$\frac{\Delta E}{\Delta t} = (\dot{m}h)_{\text{in}} - (\dot{m}h)_{\text{out}} + (\dot{m}h)_{\text{ent}} - \dot{Q}_{\text{plume-tank}} \tag{5.17}$$
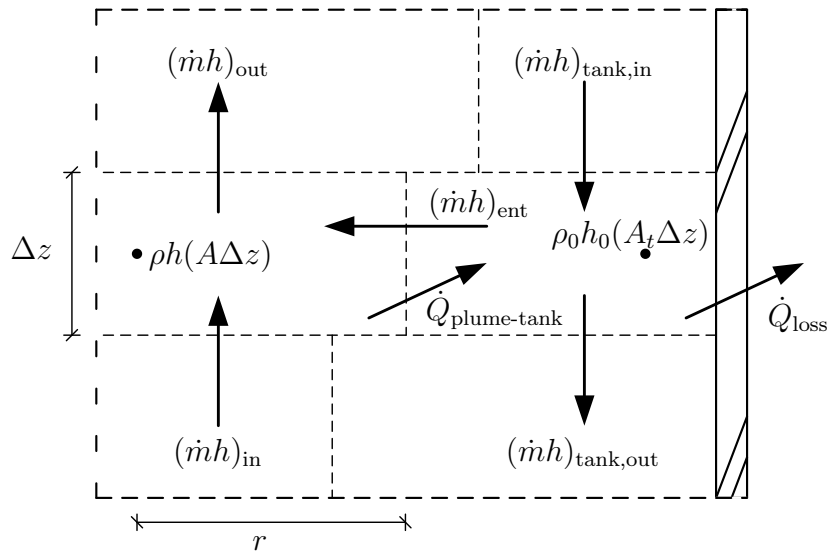
Figure 5.7: The conservation of energy on a control volume in buoyant plume

Similar to the treatment of the energy and momentum equation of the thermosyphon loop, this transient equation will be written in its explicit formulation.

First, the ΔE term is expanded.

$$\frac{(\rho A \Delta z)\,(h_{new} - h_{old})}{\Delta t} = (\dot{m}h)_{\text{in}} - (\dot{m}h)_{\text{out}} + (\dot{m}h)_{\text{ent}} - \dot{Q}_{\text{plume-tank}} \tag{5.18}$$

The enthalpy at the new time-step can then be calculated from the old values.

$$h_{new} = \frac{\Delta t}{\rho A \Delta z} \left((\dot{m}h)_{\text{in}} - (\dot{m}h)_{\text{out}} + (\dot{m}h)_{\text{ent}} - \dot{Q}_{\text{plume-tank}} \right)_{old} + h_{old} \quad (5.19)$$

The process followed above can be applied to the tank control volume in Figure 5.7 as well, yielding

$$h_{0,new} = \frac{\Delta t \left((\dot{m}h)_{\text{tank,in}} - (\dot{m}h)_{\text{tank,out}} - (\dot{m}h)_{\text{ent}} + \dot{Q}_{\text{plume-tank}} - \dot{Q}_{\text{loss}} \right)_{old}}{\rho_0 A_t \Delta z} + h_{old}$$

$$(5.20)$$

Both these explicit transient energy equations can be solved if $\dot{Q}_{\text{plume-tank}}$ and $\dot{Q}_{\text{loss}}$ are known. $\dot{Q}_{\text{loss}}$ can be calculated in a similar manner as was done for the thermosyphon loop model. Equations (4.14) to (4.19) are applied, allowing the calculation of the convective heat transfer coefficients, thermal resistances and eventually the rate of heat transfer. Also, the same method used to calculate the Nusselt number on the outside of the vertical thermosyphon tubes will once more be used on the outside of the tank.

It is further assumed that the very low velocities inside the tank prevent the usage of forced internal flow correlations. The same natural convective formula used to calculate the outside heat transfer coefficient will thus be used on the inside as well.

$\dot{Q}_{\text{loss}}$ can thus be readily calculated from formulae already introduced.

To find $\dot{Q}_{\text{plume-tank}}$, the following formula is employed.

$$\dot{Q}_{\text{plume-tank}} = \frac{T_{\text{plume}} - T_{\text{tank}}}{\text{R}_{\text{plume-tank}}} \quad (5.21)$$

Since the boundaries between the plume and tank control volumes do not really exist, but are based on an assumptions, another assumption is required to calculate $\text{R}_{\text{plume-tank}}$. The plume will be treated as forced turbulent flow within a round pipe, taking the tank temperature as the temperature of the pipe wall.

$$\text{Nu} = 0{,}023\text{Re}_{\text{D}}^{0,8}\text{Pr}^{0,3} \tag{5.22}$$

It is evident that the applicability of this is a very large assumption and will be commented on when the model is validated.

All the terms in the two transient energy equations are thus known and the new enthalpies can be found.

Finally, although not indicated in Figure 5.7, it is accepted that normal conduction of heat also takes place between all of the control volumes: within the plume, tank and the region above the thermocline, as well as between these regions.

These conductive heat transfer rates are calculated according to the formula

$$\dot{Q}_{\text{conduction}} = \frac{kA_{\text{conduction}}\Delta T}{L_{\text{conduction}}} \tag{5.23}$$

5.2.4   Summary of one-dimensional model

The complete three-part, one-dimensional, finite-volume plume model has now been derived. In summary, it consists of the following procedures. . .

- Calculate all heat transfer rates using old temperatures.

- Find the new plume and tank temperatures using the explicit transient Equations (5.19) and (5.20).

- Determine the new plume velocity field from Equation (5.10), using the new temperatures and marching from the inlet velocity.

- Calculate the new plume radii and mass flow rates from Equation (5.16), using the new temperatures and velocity field and marching from the inlet mass flow rate to the thermocline.

- Calculate all other mass flow rates from the conservation of mass.

5.3   Validation and discussion

As was discussed in the validation section of the thermosyphon loop model, validation will be done graphically.

Towards this end, the following two figures compare the model results with experimental measurements.
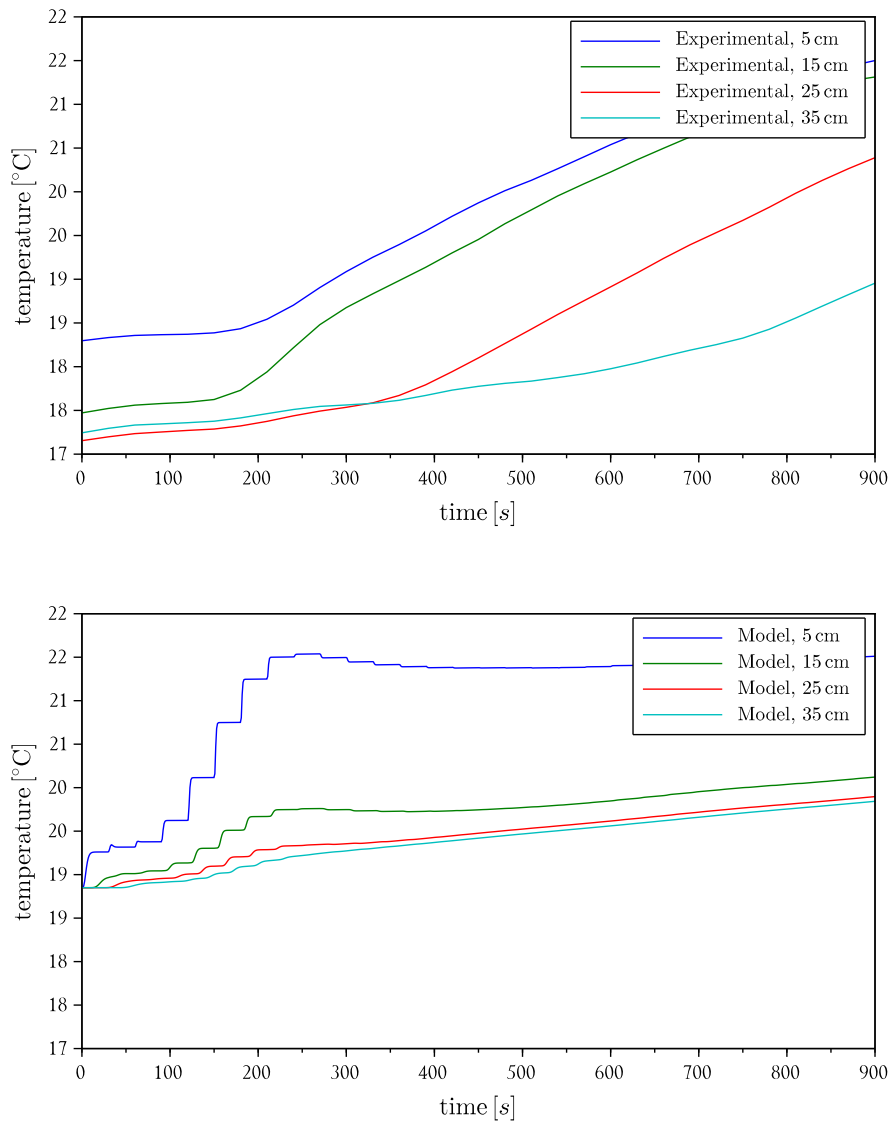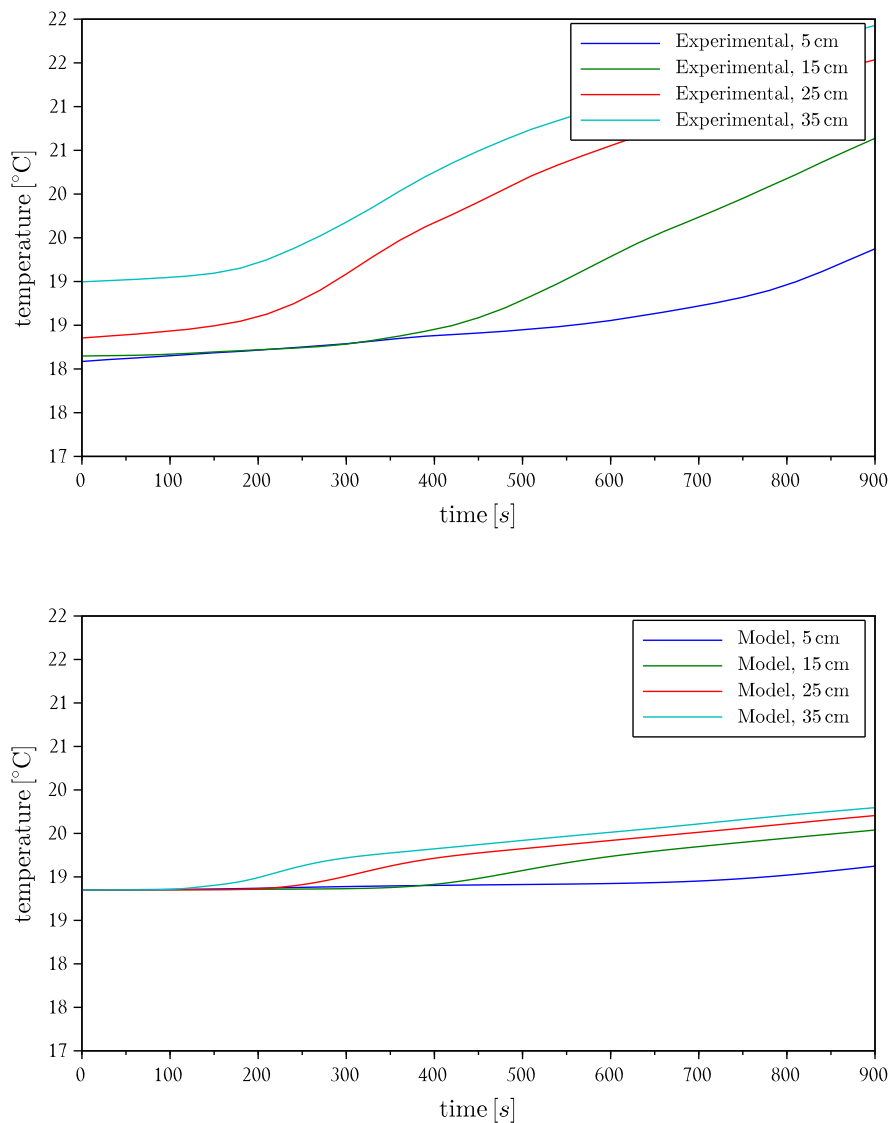

Figure 5.8: Plume temperature comparison plot

Figure 5.9: Tank temperature comparison plot

Unfortunately, it is evident from these figures that the model does not correlate well with experimental results. What it does predict, even though it does so at an incorrect magnitude, is the temperature profile along the height of the tank.

This is better seen in Figure 5.10, which is a snapshot of the tank temperatures at 900 s. This figure also includes the temperature profile predicted by two of the other models mentioned in literature.
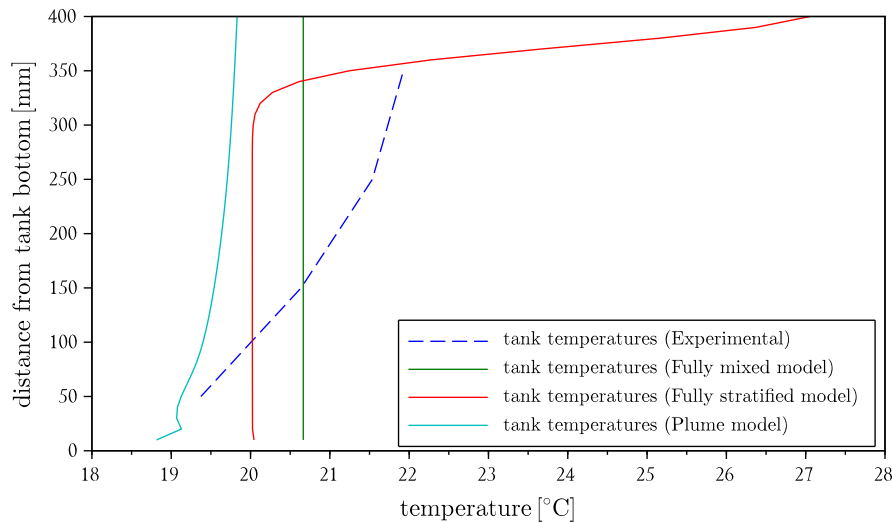
Figure 5.10: Tank temperature profiles according to different models

From the three models, it is the plume model that best captures the correct temperature profile. This is important since the degree to which stratification is achieved greatly affect the efficiency of the system.

The ability of the plume model to predict the temperature profile can be seen as proof that it does hold promise and warrants further development. It is not enough proof to validate the models correctness, however. From the data in Figures 5.8 and 5.9, it must be concluded that, at this time, the plume model is invalid.

It can further be concluded that for use in a complete solar water heating system model, the fully mixed model is suggested.

Finally, some suggestions can be made towards the improvement of the plume model.

It must be noted that the plume model heavily relies on the inlet mass flow rate. For the data presented in Figures 5.8 and 5.9, the experimentally determined mass flow rate was used as an input. This value, as was discussed, suffers somewhat from measurement error. This error will greatly affect the model. If more certain mass flow rates are thus used for an input, the model would likely produce more valid results.

Also, in calculating the heat transfer from the plume to the tank, Equation (5.22) was used. This proved (as could be expected) as an entirely invalid assumption. If the heat transfer from the plume to the tank was correctly modelled, the plume temperatures would be lower and the tank temperatures higher. This would bring the modelled temperatures closer to the measured ones. It is therefore recommended that the precise heat transfer mechanism from the plume to the tank be investigated.

Chapter 6

Conclusion and recommendations

In an attempt to seed future research and development of solar water heating technologies in Africa, the present research question was posed:

> *How well can a one-dimensional, finite-volume, computational model capture the flow inside the storage tank and piping of a thermosyphon type solar water heater?*

To answer this question, it was the goals of the present investigation to develop and validate two one-dimensional, finite-volume models. These models, that of a thermosyphon loop and of plume formation and entrainment in a HWST, were developed from first principle. This was done to encourage understanding of the subject matter among undergraduate engineering students.

The first two goals, the development and validation of the models themselves were thus partly reached – this document being the proof thereof. Specifically, the thermosyphon loop model was successfully modelled and validated. The plume model, however, proved to be invalid and in need of revision. The third goal of encouraging research cannot at this point be evaluated. It can be stated, however, that the objectives set out towards accomplishing the goal were reached, since the models were developed modularly and from first principle.

As far as the research question is concerned, the findings are positive. The validity of the thermosyphon loop model proves that a one-dimensional, finite-

volume, computational model can indeed capture the flow inside a thermosyphon type solar water heater and does so well at or near steady state.

Since the concept of using a one-dimensional, finite-volume model to simulate flow inside a solar water heater is therefore proven, much future research can be suggested.

Firstly, the current models themselves can be improved. The thermosyphon loop model can be adjusted to better capture transient flow. The experimental set-up can also be improved to better measure mass flow rate. The more reliable experimental results can then be used to further validate and improve the models, especially as far as heat transfer is concerned. As far as improving the models is concerned, however, by far the most recommended work lies in improving the plume model. Though it currently does poorly in capturing the flow, it does capture the tank temperature profile, which is what motivates further improvement and not just discarding it.

Secondly, new modules can be added to the larger model. The one-dimensional, finite-volume, from-first-principle methodology can be applied to modelling the collector and the load and cold water feed loops of the HWST.

Finally, a model of a complete thermosyphon type solar water heater can be assembled from these modules and tested against an experimental set-up. Such a model would not only enable the manipulation of several design criteria, but would also greatly improve the understanding of the system for the researchers themselves.

In conclusion, therefore, this present research has established that a one-dimensional, finite-volume model can capture the flow inside a solar water heater and does thereby encourage future work.

List of References

Abdunnabi, M.J.R. and Loveday, D.L. (2012). Optimization of Thermosyphon Solar Water Heaters Using TRNSYS . Part1 : Improved Model development and Validation. In: *2012 International Conference on Future Environment and Energy*, vol. 28, pp. 145–153. Singapore.

Anshoff, H..I. and Hayes, R. (1973). Roles of models in corporate decision making. In: Ross, M. (ed.), *Operations Research '72: Proceedings of the Sixth IFORS International Conference on Operational Research*. North Hollard:, Amsterdam.

Austin, G. and Morris, G. (2005). The status of solar water heating for domestic hot water supply in the low-income sector in South Africa. Tech. Rep., Agama Energy, Stellenbosch.

Austin, G., Williams, A., Morris, G., Spalding-Fetcher, R. and Worthington, R. (2003). Employment potential of renewable energy technology in South Africa. Tech. Rep., Agama Energy, Cape Town.

Baines, P.G. (2014). Plumes, entrainment and B.R. Morton. *Australian Meteorological and Oceanographic Journal*, vol. 64, no. 1, pp. 5–10. ISSN 1836716X.

Çengel, Y.A. and Cimbala, J.M. (2010). *Fluid Mechanics: Fundamentals and Applications*. 2nd edn. McGraw-Hill, New York.

Çengel, Y.A. and Ghajar, A.J. (2011). *Heat and Mass Transfer: Fundamentals and Applications*. 4th edn. McGraw-Hill, New York.

Cebeci, T. (1974). Laminar-Free-Convective-Heat Transfer from the Outer Surface of a Vertical Slender Circular Cylinder. In: *Proceedings of the 5th International Heat Transfer Conference*, pp. 15–19. Tokyo.

Chapman, S.J. (1998). *Fortran 90/95 for Scientists and Engineers*. WCB/McGraw-Hill, Boston. ISBN 9780070119383.

Hunt, G.R. and Kaye, N.B. (2005). Lazy plumes. *Journal of Fluid Mechanics*, vol. 533, pp. 329–338. ISSN 0022-1120.

Hunt, G.R. and van den Bremer, T.S. (2011). Classical plume theory: 1937–2010 and beyond. *IMA Journal of Applied Mathematics*, vol. 76, no. 3, pp. 424–448.

Kaye, N.B. (2008). Turbulent Plumes in Stratified Environments: A Review of Recent Work. *Atmosphere-Ocean*, vol. 46, no. 4, pp. 433–441. ISSN 0705-5900.

Le Fevre, E. (1956). Laminar Free Convection from a Vertical Plane Surface. In: *Proceedings of the 9th International Congress on Applied Mechanics*, p. 168. Brussels.

Maclaren, N. (2010). Software Design and Development.

Morrison, G. and Braun, J. (1985). System modeling and operation characteristics of thermosyphon solar water heaters. *Solar Energy*, vol. 34, no. 4-5, pp. 389–405. ISSN 0038092X.

Morrison, G. and Ranatunga, D. (1980*a*). Thermosyphon circulation in solar collectors. *Solar Energy*, vol. 24, no. 2, pp. 191–198. ISSN 0038092X.

Morrison, G. and Ranatunga, D. (1980*b*). Transient response of thermosyphon solar collectors. *Solar Energy*, vol. 24, no. 1, pp. 55–61. ISSN 0038092X.

Morrison, G. and Tran, H. (1984). Simulation of the long term performance of thermosyphon solar water heaters. *Solar Energy*, vol. 33, no. 6, pp. 515–526. ISSN 0038092X.

Morton, B.R., Taylor, G. and Turner, J.S. (1956). Turbulent Gravitational Convection from Maintained and Instantaneous Sources. *Proceedings of the Royal Society A: Mathematical, Physical and Engineering Sciences*, vol. 234, no. 1196, pp. 1–23. ISSN 1364-5021.

Naylor, T. and Finger, J. (1967). Verification of computer simulation models. *Management Science*, vol. 14, no. 2.

Oberkampf, W.L. and Trucano, T.G. (2008). Verification and validation benchmarks. *Nuclear Engineering and Design*, vol. 238, no. 3, pp. 716–743. ISSN 00295493.

Ong, K. (1974). A finite-difference method to evaluate the thermal performance of a solar water heater. *Solar Energy*, vol. 16, no. 3-4, pp. 137–147. ISSN 0038092X.

Ong, K. (1976). An improved computer program for the thermal performance of a solar water heater. *Solar Energy*, vol. 18, no. 3, pp. 183–191. ISSN 0038092X.

Ostrach, S. (1952). An analysis of laminar free-convection flow and heat transfer about a flat plate parallel to the direction of the generating body force. Tech. Rep..

Popiel, C.O. (2008). Free Convection Heat Transfer from Vertical Slender Cylinders : A Review. *Heat Transfer Engineering*, vol. 29, no. June, pp. 521–536.

Rani, N., Setia, H., Dutt, M. and Wanchoo, R.K. (2014). Natural Convection Heat Transfer from Inclined Cylinders : A Unified Correlation. *International Journal of Mathematical, Computational, Physical, Electrical and Computer Engineering*, vol. 8, no. 1, pp. 100–105.

Roy, C.J. and Oberkampf, W.L. (2011). A comprehensive framework for verification, validation, and uncertainty quantification in scientific computing. *Computer Methods in Applied Mechanics and Engineering*, vol. 200, no. 25-28, pp. 2131–2144. ISSN 00457825.

Sargent, R. (2013). Verification and validation of simulation models. *Journal of Simulation*, vol. 7, no. 1, pp. 12–24. ISSN 1747-7778. 10.

Sargent, R.G. (1981). An assessment procedure and a set of criteria for use in the evaluation of computerized models and computer-based modeling tools. Tech. Rep., U.S. Air Force.

Sargent, R.G. (1986). The use of graphical models in model validation. In: Wilson, J.R., Henriksen, J..O. and Roberts, S.D. (eds.), *Proceedings of the 1986 Winter Simulation Conference*. Piscataway.

Scase, M.M., Caulfield, C.P., Dalziel, S.B. and Hunt, J.C.R. (2006). Time-dependent plumes and jets with decreasing source strengths. *Journal of Fluid Mechanics*, vol. 563, p. 443. ISSN 0022-1120.

Solar Energy Laboratory (2009). TRNSYS 17. Tech. Rep., Solar Energy Laboratory.

Taylor, G. (1945). Dynamics of a mass of hot gas rising in air. Tech. Rep., U.S. Atomic Energy Commission.

Turner, J.S. (1986). Turbulent entrainment: the development of the entrainment assumption, and its application to geophysical flows. *Journal of Fluid Mechanics*, vol. 173, no. -1, p. 431. ISSN 0022-1120.

Wlokas, H.L. and Ellis, C. (2013). Local employment through the low-pressure solar water heater roll-out in South Africa. Tech. Rep., University of Cape Town: Energy Research Centre, Cape Town.

Woods, A.W. (2010). Turbulent Plumes in Nature. *Annual Review of Fluid Mechanics*, vol. 42, no. 1, pp. 391–412. ISSN 0066-4189.

Ziapour, B.M. and Aghamiri, A. (2014). Simulation of an enhanced integrated collector–storage solar water heater. *Energy Conversion and Management*, vol. 78, pp. 193–203. ISSN 01968904.